Imprints of volcanic, erosional, depositional, tectonic and mass-wasting processes in the morphology of Santa Maria insular shelf (Azores).

Title: Imprints of volcanic, erosional, depositional, tectonic and mass-wasting processes in the morphology of Santa Maria insular shelf.

Alessandro Ricchi[a], Rui Quartau[b,c], Ricardo S. Ramalho[c,d,e,f], Claudia Romagnoli[a], Daniele Casalbore[g,h], Zhongwei Zhao[i]

[a]University of Bologna, Dip. Scienze Biologiche, Geologiche e Ambientali, Bologna, Italy
[b]Instituto Hidrográfico, Divisão de Geologia Marinha, Lisboa, Portugal
[c]Instituto Dom Luiz, Faculdade de Ciências, Universidade de Lisboa, Lisboa, Portugal
[d]Departamento de Geologia, Faculdade de Ciências, Universidade de Lisboa, Lisboa, Portugal
[e]School of Earth Sciences, University of Bristol, Bristol, UK
[f]Lamont-Doherty Earth Observatory at Columbia University, Palisades, NY, USA
[g]Istituto di Geologia Ambientale e Geoingegneria, Consiglio Nazionale delle Ricerche, Area della Ricerca, Roma, Italy
[h]Sapienza Università di Roma, Dipartimento Scienze della Terra, Roma, Italy
[i]Department of Earth and Environmental Sciences, University of Manchester, Williamson Building, Oxford Road, Manchester M13 9PL, UK.

Corresponding author: Rui Quartau (rui.quartau@hidrografico.pt)

Highlights: (85 characters)

- The wider northern shelf suggests that the island might be older than 6 Ma
- The shelf is mostly sediment-deprived, except in fault-controlled basins
- Depositional sequences in island shelves are hard to preserve due to wave exposure
- Mass wasting at the shelf edge is driven by tectonics and sediment accumulation

Abstract

The present-day morphology of volcanic island shelves is the result of several factors, namely the original shape and structure of the volcanic edifice, the nature and age of the materials that compose its flanks, and the erosional, volcanic, tectonic and sedimentary processes that acted to form these shelves. By combining detailed seafloor mapping with onshore studies it is possible to gain a unique insight onto the evolution of volcanic island edifices and the processes that helped to shape their shelves. Here we look at Santa Maria Island in the Azores Archipelago, which is a 6 Ma old ocean-island volcano surrounded by a 135 km^2 shelf, characterized by an history of subsidence since its formation c. 6 Ma ago, followed by uplift from 3.5 Ma onwards. By analyzing the geomorphic parameters of the insular shelf (such as the shelf width and the erosive edge depth), the island's history of vertical movements, and by relating the morphology of the outcrops found on the shelf with those onshore, we contribute to a better knowledge of the evolutionary history of Santa Maria with particular focus on its earlier stages of growth. We infer that the outer part of the northern shelf is carved on units older than the oldest volcanic sequences exposed on land; the western and southern shelves are almost entirely carved in the products of the oldest shield volcano (Anjos Volcanic Complex), whilst the eastern shelf is the youngest in formation, being related to units of the Pico Alto volcanic complex. We also discuss the distribution of sediments on the shelf. High wave energy concomitant with sea level drops contributed to the erosion and transport of older sequences offshore, which were ultimately lost to the slopes of the island, resulting in a shelf that is sediment-stripped for the most part. Presently, wide shelves further contribute to wave-energy dissipation, resulting in a significantly diminished sediment production. The shelf edges around Santa Maria exhibit several erosive scars, interpreted as the head of a submarine drainage network carved on the slopes of the island. On the western,

25 southern and eastern shelves, these mass-wasting features are mostly controlled by tectonics
26 since the extension of faults and lineaments can be followed from onshore to the shelf edge. On
27 the northern shelf mass-wasting appears to be mostly correlated with presence of unstable
28 sediments on the shelf edge that triggered landsliding. Overall, this work shows how detailed
29 mapping of the shelves surrounding old volcanic islands can still provide important
30 complementary information about the evolution of these islands, which could not be acquired
31 solely by the study of their subaerial and deeper submarine parts.

1. Introduction

The subaerial and submarine morphology of volcanic islands results from the interplay between volcanic, tectonic, erosive and depositional processes acting at different time-scales (Ramalho et al., 2013; Casalbore et al., 2015; Lebas et al., 2018; Quartau et al., 2018a). These processes and their influence on the geomorphology are very well known for the subaerial portions of volcanic islands (e.g., Thouret, 1999). However, volcanic islands are mostly developed beneath the sea; hence the study of their submarine areas can provide much more information than the subaerial parts, which constitute only the "tip of iceberg" (e.g., Quartau and Mitchell, 2013; Quartau et al., 2015a). Most part of submarine studies was mainly addressed to reconstruct large-scale instability processes that commonly affect the flanks of these edifices (Moore et al., 1989; Deplus et al., 2001; Masson et al., 2002; Mitchell et al., 2002; Oehler et al., 2008; Casalbore et al., 2011; Montanaro and Beget, 2011). On the contrary, less attention has been paid on the impact of volcanism, erosion, tectonics, time-variant sediment supply and climatic/oceanographic conditions on the surrounding shelves and the link with the geology onshore. Only in the last decade, a few number of nearshore marine surveys performed with high-resolution multibeam and seismic reflection systems revealed the importance of insular shelf studies to obtain a more detailed picture of the geological history of volcanic islands (Quartau et al., 2012; Romagnoli, 2013; Quartau et al., 2014; Quartau et al., 2015b; 2016; Casalbore et al., 2018; Ricchi et al., 2018; Romagnoli et al., 2018). Insular shelves surrounding volcanic islands are, in fact, representative of their original subaerial extension during glacial maxima, thus playing a potential role for palaeo-morphological and relative age reconstructions as well as for evaluating the vertical mobility of such areas (Lucchi et al., 2019; Quartau et al., 2016, 2018b; Ricchi et al., 2018). Geomorphic parameters such as the shelf edge depth and shelf width, as well as the morphology of the submerged lava flows or rocky outcrops, provide useful insights concerning the original

morphology of the volcanic edifices, and the occurrence of (older or younger than expected) volcanic activity not recorded onshore (Quartau et al., 2014; 2015b; Ramalho et al., in press; Romagnoli et al, 2018). For instance, shelf width can be related with shelf age (beginning of incision) and as such may be used to infer reveal relative ages of undated coastal sectors (Quartau et al., 2010; Romagnoli et al, 2018). In a similar fashion, coastal sectors formed by volcanism with similar ages but different orientations to waves generally exhibit different shelf widths and may thus reveal that wave regimes have probably not changed through time (Llanes et al., 2009; Mitchell et al, 2003; Quartau et al., 2010). Erosional shelf breaks which are now deeper than the lowest sea-level stands, may also be related with subsidence of the volcanic edifices and thus rates of vertical movements can also be estimated from the depth of the shelf break (Lucchi et al., 2019; Quartau et al., 2014, 2016, 2018b), in a similar way that constructional slopes breaks were used in Hawaii to estimate subsidence and relative age constraints of volcanic edifices (Taylor, 2019). To date, however, only a few studies have discussed sediment deposition on volcanic island shelves and the preservation of their depositional sequences (Ávila et al., 2008; Casalbore et al., 2018; Meireles, 2013; Quartau et al., 2012). Moreover, all the existing shelf studies have focused on relatively young islands (~1 Ma or less). At Santa Maria, however, there there is the opportunity of looking into a much older island (~6 Ma) and test whether the approaches and interpretation taken from younger islands could also apply to older edifices. In addition, Santa Maria's shelf is up to now, one of the best surveyed insular shelves in the world, with a cover of multibeam bathymetry of 1 m resolution and a grid of high-resolution seismic profiles not spaced more than 250 m. This opportunity provides a unique and more detailed, careful analysis on the factors that impact shelf evolution and sedimentary dynamics in an energetic environment such as the Azores.

In this study, we combined high-resolution geophysical dataset with detailed onshore geological field studies performed on Santa Maria Island (Azores Archipelago) to better

49 understand the connection between the onshore and the offshore domain. This allows
50 unprecedented inferences on the contribution of tectonics, wave regime, volcanism, erosion and
51 sediment supply in shaping the insular shelf. Moreover, through the analysis and comparison of
52 the shelf width, shelf edge depth and morphology for each sector of the island, a better
53 understanding of the evolution of Santa Maria is derived.
54

55 ## *2. Geological setting*

56

57 ### *2.1 The Azores Archipelago*

58 The Azores Archipelago is located in the North Atlantic Ocean, on both sides of the Mid-Atlantic
59 Ridge (MAR in Fig. 1), which separates the westernmost group of islands from the central and
60 easternmost groups. Volcanism here possibly results from the interaction between the triple
61 junction of the Eurasian, Nubian and American lithospheric plates and a hotspot (Gente et al.,
62 2003). The complex interaction between the seafloor spreading forces driven by the Mid Atlantic
63 Ridge and the right-transtensional movements associated with the Nubian/Eurasian plate's
64 boundary dominates the area (Lourenço et al., 1998; Hipólito et al., 2013; Marques et al., 2013;
65 Madeira et al., 2015). Santa Maria sits at the SE corner of a roughly triangular shaped area located
66 between the Nubian/European plate boundary (the active Terceira Rift, TR in Fig. 1) and the
67 presently inactive East Azores Fracture Zone (EAFZ in Fig. 1), most likely already outside the
68 influence of the Nubian/European plate boundary (Miranda et al., 2018).
69 Being under an oceanic regime, the coastlines of the Azores Archipelago are frequently subjected
70 to high wave energy. The North Atlantic Oscillation and Eastern Atlantic atmospheric circulation
71 bring extreme storms (wave heights exceeding 16 m and peak periods exceeding 18 s) affecting
72 the Azores at least once every seven years (Andrade et al., 2008; Zhao et al., 2019). For instance,

the recent Hurricane Lorenzo impacted the Azores in October 2019, with wave heights yielding 15 m that violently destroyed the port of Lajes on Flores Island, western Azores (Hatton, 2019).

2.2 Geology of Santa Maria Island

Santa Maria Island rises from the seafloor at around -2500 m and it is considered the oldest island of the Azores Archipelago, since it emerged from the sea c. 6 Ma ago (Ramalho et al., 2017). The eastern (leeward) side of the island exhibits a rugged morphology, culminating in the Pico Alto high (587 m in elevation, Fig. 2). In this sector, the coastline is made of up to 250-300 m high plunging cliffs, occasionally displaying wave-cut notches at varying elevations. On the contrary, the western (windward) side has a typical staircase morphology due to the occurrence of a number of raised marine terraces from 7 m to 200 m in elevation, some of which still exhibit remains of coastal sediments (Ramalho et al., 2017). Offshore, Santa Maria is surrounded by a wide insular shelf, in particular along the northern coastal sector (up to 8 km wide), in contrasts with narrower shelves at the western, southern and eastern sides (~2 km). Five sets of submerged marine terraces have been recognized on the shelf, reflecting the interplay between the island's vertical movements and sea-level fluctuations (Ricchi et al., 2018).

The volcanic history of Santa Maria is the result of the activity of different overlapping volcanoes, interrupted by relative long periods of quiescence and erosion (Serralheiro et al., 1987; Serralheiro and Madeira, 1993; Ramalho et al., 2017). The volcanism of the Cabrestantes and Porto Formations on the westernmost side of the island (Fig. 2), emplaced by surtseyan and strombolian activity, witnesses the first emergence of the island and transition to a subaerial volcanic edifice c. 6 Ma ago. The products of the Anjos Volcanic Complex are widespread in the central and western portions of the island, representing the remnants of a large shield volcano formed between 5.8 Ma and 5.3 Ma (Fig. 2) (Sibrant et al., 2015; Ramalho et al., 2017). The

97 following 1 Ma was mostly characterized by marine erosion that caused the partial dismantling,
98 and possibly submersion of the previously formed shield volcano. A collapse of the eastern flank of
99 the Anjos volcanic edifice has also been proposed by Sibrant et al (2015). Simultaneously with
100 marine sedimentation on top of the eroded volcano, which probably constituted a wide shoal with
101 some residual subaerial reliefs, low-volume submarine volcanism took place, mainly focused on
102 the eastern portion of the island (Ramalho et al., 2017). This culminated in the emplacement of
103 the Touril Volcano-sedimentary Complex between 5.3 Ma and 4.1 Ma (Fig. 2). During this period
104 the island experienced a subsidence trend (c. 100 m/Myr on average) that lasted until 3.5 Ma as
105 attested by the numerous passage zones of Pico Alto and Anjos lava deltas (which indicate
106 increasingly higher relative paleo sea levels towards the top of the sequence) and the
107 transgressive sequences of Touril complex showing a deepening-up sequence (Ramalho et al.,
108 2017). Widespread volcanic activity resumed c. 4.1 Ma, promoting the re-emergence of the island
109 edifice. The products of the Pico Alto volcanic complex (Fig. 2) correspond to the lateral growth of
110 the edifice due to lava delta progradation over the Touril marine sediments and the eroded
111 remains of the Anjos edifice. Subsidence reversed into uplift at 3.5 Ma (estimated at c. 59 m/Myr
112 from 3.5 Ma to 2.14 Ma and 42 m/Myr from 2.14 Ma to present), as attested by the position of
113 the passage zone of Pico Alto's lava deltas (up to 200 m), and the occurrence of marine terraces on
114 the western side of the island and offshore (Ramalho et al., 2017; Ricchi et al., 2018). Although the
115 last stage of the island evolution is considered mainly erosional, from 3.2 to 2.8 Ma a low volume
116 of magmatic and hydromagmatic activity led to the formation of the cones and products of the
117 last post-erosional phase, roughly corresponding to the Feteiras Formation of Serralheiro et al.
118 (1987) or the Young Parasitic Cones of Sibrant et al. (2015) (Fig. 2).
119 Tectonics is expressed onshore by the main NW–SE, N-S and NE–SW-trending faults (Fig. 2,
120 Madeira et al., 2015) that partly influenced the development of the subaerial terraces and

submerged terraces on the shelf (Ricchi et al., 2018). Moreover, Zbyszewski and Ferreira (1960) and Serralheiro et al. (1987) reported a large set of N 045° and N 150° striking dikes located mostly in the SW and NE portion of the island (Fig. 2), being likely contemporaneous to the main building stages of the island.

Santa Maria is the driest island in the Azores, with the low western half exhibiting between 670 and 800 mm/ year of precipitation and the more rugged and taller eastern side reaching higher values, between 1100-1700 mm/year (Fernandes, 2004).

2.3 Sedimentary dynamics at reefless Volcanic Ocean Islands

On reefless volcanic islands the production of sediments reaching the coast largely depends on volcanic activity (for instance explosive volcanism produces much more clastic materials than effusive volcanism), the occurrence of a well-developed subaerial drainage system, wet climate stimulating the subaerial erosion, and high wave energy promoting coastal erosion and sediment redistribution (Krastel et al., 2001; Ramalho et al., 2013; Quartau et al., 2018a). In particular, on small and relatively dry reefless volcanic islands (like Santa Maria), sediment is produced mainly through the erosion of coastal cliffs by wave processes because rivers do not have enough area to develop and the low precipitation imprints a weak fluvial erosion regime (Quartau et al., 2012). Thus, on these islands, sediments that result from cliff erosion accumulate in the inner shelf and are partly transported offshore during storms. Several studies showed, in fact, that storms are able to produce storm-induced downwelling currents that transport sediments from shallow to deeper areas of the shelf (Field and Roy, 1984; Tsutsui et al., 1987; Hernández-Molina et al., 2000; Chiocci and Romagnoli, 2004; Meireles et al., 2013). These sediments tend to form clinoform deposits, as recognized on other volcanic islands of the Azores (Quartau et al., 2012; 2014; 2015b) and in the

145 Mediterranean Sea (where they are named "submerged or submarine depositional terraces",
146 Chiocci and Romagnoli, 2004; Casalbore et al., 2017; Romagnoli et al., 2020).
147
148 ## *3. Material and methods*
149
150 ### *3.1 Shelf data acquisition and processing*
151 The shelf around Santa Maria Island has been surveyed onboard the R/V *Arquipélago* from 24th
152 August to 15th September 2016 in the scope of PLATMAR project. The survey (PLATMAR 1/2016)
153 included the acquisition of multibeam bathymetry and single-channel seismic profiles (boomer)
154 between c. -20 m and c. -250 m (Figs. 3 and 4). Further details of the geometry acquisition and
155 equipment were reported by Ricchi et al. (2018). The subaerial DTM was generated from a 1/5000
156 scale digital altimetric database with a resolution of 5 m. An integrated analysis of the multibeam
157 bathymetry and subaerial topography has been mainly used to study the morphology of the shelf
158 by mapping the volcanic, structural, erosional and depositional features and comparing with those
159 of the corresponding onshore sectors (Figs. 4, 5a, 6a, 7a, 8a and 1ESM). The shelf width and the
160 erosive edge depth values in each sector were determined from the seismic profiles collected
161 perpendicular to the coastlines (Fig. 3) and reported in graphs in order to constrain its variability
162 along the shelf (Figs. 5a, 6a, 7a and 8a). The erosive shelf edge was defined as the point, in the
163 rocky basement of the seismic profiles, where there is a significant increase in gradients to the
164 slope of the island (e.g., Fig. 2ESM). Shelf width was only measured where erosive shelf edge and
165 coastlines stretches were roughly parallel to each other, whilst shelf edge depth was measured
166 along the entire shelf. Since mass wasting of the shelf edge can cause a landward shift of that
167 feature and shallow its depth, we always took into account in our interpretation areas without
168 scars, which is considered to represent the original depth at which waves cut the island subaerial

169 flanks. The analysis of seismic reflection profiles allowed mapping the distribution and thickness of
170 the unconsolidated sediments lying on the shelf of Santa Maria Island (Fig. 9 and Table 1). In each
171 seismic profile we picked two reflectors corresponding to the seafloor and, where present, the
172 bottom of the sedimentary cover, respectively. For time/depth conversion we used a sound
173 velocity of 1500 m/s for the water column and 1800 m/s for the sediments. Sound velocity is
174 based on data of Hamilton and Bachman (1982) for coarse sands, which in the Azorean shelves are
175 the dominant grain-size (Quartau et al., 2012; Quartau et al., 2015b).
176
177 ***3.2 Wave regime characterization***
178 Using the model outputs of the European Centre for Medium range Weather Forecasts
179 (ECMWF) 40-yr Re-Analysis (ERA-40) (Uppala et al., 2005) and ECMWF Interim Re-Analysis (ERA-
180 Interim) (Dee et al., 2011), a rose diagram for Santa Maria offshore significant wave heights (and
181 their associated percentages and originating directions was produced (Figure 10, Table 1ESM).
182 These wave properties were extracted from a six hourly significant wave height H_s database and
183 averaged for the sea area adjacent to Santa Maria Island (36.875°N - 37.125°N, 24.9375°W –
184 25.25°W) for the period September 1957 to August 2019 and represent the base for discussing the
185 the wave regime in the different shelf sectors.
186
187 ## *4. Results*
188
189 ### *4.1 Morphology of the insular shelf around Santa Maria Island*
190 #### *4.1.1 Northern shelf sector*
191 This sector is located offshore the northern coast of the island from Baía do Mar da Barca to
192 Ponta do Norte (A to B in Fig. 5a). The roughly ENE-WSW oriented coastline has a strongly irregular

193 profile characterized by embayments and promontories. From Ponta do Norte to Ponta dos
194 Frades, sea cliffs are steep, up to 200 m high, and were cut in the products of the Anjos Volcanic
195 Complex at the base, overlapped by those of Touril Volcano-sedimentary and Pico Alto Volcanic
196 Complex (see Fig. 2), forming a tabular sequence, dipping very gently to the eastern quadrant.
197 From Ponta dos Frades to Baía do Mar da Barca, cliffs are entirely carved in the products of the
198 Anjos Volcanic Complex and their height progressively decreases westwards to ~20-30 m. The
199 entire shelf has a roughly trapezoidal shape and shows a different morphology between the
200 eastern and the western sides, similarly to the asymmetric topography of the island. To the east of
201 Ponta dos Frades the shelf width varies between 6 km and 8 km, while to west is narrower being c.
202 4 km wide (not considering the sector where the submarine cone of Baixa do Ambrósio is located,
203 Figs. 5a and 5b). The maximum depth of the erosive shelf edge is c. 170 m on the northwestern
204 portion (off Baía do Mar da Barca, Figs. 5a and profile aa' in Fig. 2ESM), then it slowly decreases to
205 156 m to the north and increases again up to 172 m in the northeast. Depth values as low as c. 115
206 m can be found, corresponding to scars affecting the shelf edge.
207 To the west of Ponta dos Frades, rocky outcrops have been recognized down to a depth of 80-
208 100 m, being mostly located in the inner to middle shelf. These are cut by sharp linear
209 escarpments, ranging in heights from c.10 m to c.30 m in three compartmented blocks (Fig. 5a).
210 These lineaments, 2 to 2.7 km long, can be followed from the subaerial island into shallow water
211 and down to -100 m, where they apparently disappear in an area characterized by an overall
212 smooth morphology. Offshore continuation of these lineaments is possibly represented by a sharp
213 escarpment that dissects a rocky outcrop located to the south of Baixa do Ambrósio at c.-130/-170
214 m (probable extension of AjF in Fig. 5a) and by a narrow gully head, located SE of Baixa do
215 Ambrósio at -135 m (probable extension of CF in Fig. 5a). To the east, another lineament (RF in Fig.
216 5a) can be also apparently followed offshore in a NNW-SSE linear escarpment c. 2 km long, down

217 to -50 m. These major lineaments are in clear connection with recognized fault
218 planes/escarpments on land, as they are more evident in the case of the Aeroporto and Anjos
219 Faults (AF and AjF in Fig. 5a and profile cc' in Fig. 3ESM).

220 To the east of Ponta dos Frades, the entire shelf is dominated by rocky outcrops with some sub-
221 conical or elongated morphological highs. A total of 26 sub-conical structures were recognized
222 from c. -70 m to c. -120 m on this shelf sector (Fig. 5a). These morphological features show a
223 random arrangement on the shelf and exhibit different sizes and morphologies. Four types of sub-
224 conical landforms were identified in this sector: a) small conical, circular or elongated, positive
225 relief (numbers 1–9 in Fig. 5a); b) larger, more irregular and concentric morphologies with positive
226 relief and sometimes a flat or depressed top, and with a basal diameter from c. 0.25 km to c. 1 km
227 and heights comprehended between c. 20 m and c. 40 m (numbers 10–18 in Fig. 5a); c) large
228 roughly-circular features with a wide central depression, ranging from 800 m to 1.2 km in width
229 and up to 30 m in height (numbers 19–23 in Fig. 5a); and d) small round-to-elliptical ring-like
230 features, up to c. 600 m in diameter and 15 m high, with an internal depressed area covered by
231 sediments (numbers 24 and 25 in Fig. 5a). A large elliptical elevation (Baixa do Ambrósio, 1.3 km in
232 diameter and about 130 m high) also stands prominently isolated on the NW portion of this shelf
233 sector. This is a popular recreational diving site and submarine photos of this area abound. These
234 show that this morphology is a pillow-lava cone whose flanks are cut by marine terraces located at
235 different depths (Ricchi et al., 2018). In addition to the conical morphologies, a prominent NNW-
236 SSE rocky ridge can be seen in the central-eastern part of the shelf, extending from the coastline
237 to the shelf edge, almost exactly in line with the Pico Alto ridge onshore (see arrow in Fig. 5a and
238 compare it to Fig. 2). Along this submarine ridge, several N-S linear positive reliefs are present also
239 in line with dykes exposed at the coast (see Fig. 4 and 1ESM), in between Lagoínhas and Ponta do
240 Pesqueiro Alto (Fig. 2) (Zbyszewski and Ferreira, 1960; Madeira, 1986; Madeira et al., 2015).

241 In terms of surface area, the sedimentary cover amounts almost the same as the sediment-free
242 rocky surfaces, i.e., around 50% each (see Table 1). A total of 0.515 km^3 of sediments are
243 deposited on this sector and the ratio volume of sediments/shelf surface area is 0.007. Sediments
244 are mostly restricted to the outer part of shelf in the NW and in-between the rocky outcrops in the
245 NE (Fig. 9). Deposits are normally very thin (mostly between 0 and 2 m), being locally thicker (up to
246 14 m) on local depocenters bordered by sub-vertical escarpments (e.g., the NW-SE oriented small
247 basin located offshore Baia da Cré, and the ENE-WSW oriented basin offshore Ponta do Norte -
248 see Fig. 9 and seismic profiles bb' and cc' in Fig. 3ESM).
249
250 ***4.1.2 Western shelf sector***
251 This sector is located offshore the western coast of the island from Baía do Mar da Barca to
252 Ilhéu da Vila (Fig. 6a). The coastline is NNW-SSE oriented with sub-vertical sea cliffs up to 75 m
253 high, entirely carved in the subaerial westward-dipping lava flows and pyroclastic succession of the
254 Anjos Volcanic Complex (Fig. 2). The shelf runs parallel to the coastline and is generally rocky down
255 to c. -50/-70 m. Offshore Campo Grande a NW-SE strip of sedimentary seafloor (Fig. 6a and 9)
256 around 1.7 km long and c. 150 m wide separates the shelf in two parts characterized by different
257 widths (c.1.2-1.6 km to the north, c.2 km to the south). In this sector the erosive shelf edge is
258 generally at -100/-110 m along the northern portion, whilst in the southernmost part its depth
259 increases to -135/-147 m (Figs. 6a, 6b and profile dd' in Fig. 4ESM). However, between offshore
260 Campo Grande and Ponta do Poção, the shelf edge has been indented, shallowing its depth up to -
261 50 m.
262 The lineament located offshore Campo Grande exhibits onshore an arc-shaped escarpment
263 dissected by a set of WNW-ESE and WSW-ENE structures and the Campo Grande fault (CgF in Fig.
264 6a, Madeira et al., 2015). In this whole area, the rocky outcrops seen in the high-resolution

bathymetry are frequently cut by these WNW-ESE and WSW-ENE lineaments (see figure ESM1), which are parallel to the dike network seen on the adjacent coast (Zbyszewsky and Ferreira, 1960; Madeira, 1986; Madeira et al. 2015). In a similar fashion, a few well-pronounced NNW-SSE to NNE-SSW lineaments can be seen cutting the rocky shelf in this area, running approximately parallel to shore and to the Aeroporto Fault further inland (Fig. 4, AF in Fig. 6a and Fig. 1ESM).

The surface of the seafloor in this sector corresponds to ~75% of rocky surfaces and 25% of sedimentary cover (Table 1). It has total of 0.037 km^3 of sediments and the ratio volume of sediments/shelf surface area is 0.003. Sediments are therefore restricted to a few scattered patches at -100/-120 m. These are also present inside the WNW-ESE oriented lineament offshore Campo Grande, with thicknesses less than 5 m, which increase up to c. 10 m at the shelf edge (Fig. 9).

4.1.3 Southern shelf sector

This sector is located offshore the southern coast of the island from Ilhéu da Vila to Ponta do Castelo (Fig. 7a). In the western-most portion to Ponta da Marvão, the coastline is very irregular in plan-view, with cliffs mostly formed by SW-dipping lava flows and pyroclastic products of the Anjos Volcanic complex (Fig. 2). From Ponta da Marvão to Ponta do Malbusca, the coastline exhibits an arcuate shape due to the occurrence of a 6 km-wide bay (Praia Formosa Bay, Fig. 7a), bounded by up to 200 m-high, sub-vertical sea cliffs. These are cut in a sequence comprising the Anjos Volcanic Complex lava flows at the base, overlapped by marine sediments and submarine/subaerial volcanic products of both the Touril and the Pico Alto Volcanic Complexes (Fig. 2). From Ponta da Malbusca to Ponta do Castelo the coastline is made of steep cliffs, carved on the Touril and Pico Alto sequences (Fig. 2).

The southern shelf has an irregular morphology, with its edge showing a configuration that roughly mimics the coastline west of Ponta da Malbusca. The westernmost portion of the shelf is around 2 km wide, up to the eastern end of Praia Formosa Bay, after which it is reduced to c. 1 km offshore Ponta da Malbusca. Eastwards it enlarges again, increasing to up to 2.6 km in width offshore Ponta do Castelo, at the SE edge of the sector (Figs. 7a and 7b). The depth of the erosive shelf edge follows a similar trend, i.e., deeper where the shelf is wider and shallower when it is narrower. Between south of Ilhéu da Vila to Praia Formosa Bay it is 80/90 m (although can reach 120 m in places), while it is in the range of 50/90 m at Ponta da Malbusca. Then, the shelf edge depth progressively increases to a maximum value of 142 m offshore Ponta do Castelo (Figs. 7a, 7b and profile ee' in Fig. 5ESM).

A dense network of NNW-SSE and NNE-SSW trending lineaments, 0.5 km to 2 km long and with escarpments up to 15 m high, dissects the shelf from the coastline down to its edge, creating a succession of rocky structural high interspersed by sediment-covered depressed areas (Figs. 7a, 9 and seismic profile ff' in Fig. 6ESM). The most evident features are located offshore Vila do Porto, Praia Formosa Bay and Ponta da Malbusca, also having a clear morphological expression onshore (Fig. 7a). The lineaments that compartmentalize the shelf show an orientation similar to the dike network exposed all along this stretch of coastline (see Zbyszewsky and Ferreira, 1960 and Madeira, 1986), (Fig. 7a) and, in some cases, can be followed to the outer shelf. The western Fault of Malbusca (FM in Fig. 7a) also continues offshore, as expressed by a small NNE-SSW linear escarpment.

The distribution of sedimentary cover and rocky surfaces is very similar to the northern sector, around 50% each (Table 1). This shelf sector has a total of 0.221 km^3 of sediments and a ratio volume of sediments/shelf surface area of 0.012. The distribution of the sediments and their thickness is highly variable being from <6 m (offshore Ilhéu da Vila) up to 15-20 m (offshore Praia

312 Formosa Bay, Fig. 9, seismic profile ff' in Fig. 6ESM and seismic profile gg' in Fig. 7ESM). Offshore
313 Praia Formosa and west of Ponta da Malbusca the sediments cover most of the shelf, whilst
314 offshore Ilhéu da Vila and from Ponta do Malbusca to Ponta do Castelo the sediments cover only
315 the outer shelf with a gradually decreasing thickness towards the shelf edge (Fig. 9).
316
317 ***4.1.4 Eastern shelf sector***
318 This sector is located offshore the eastern coast of the island from Ponta do Castelo to Ponta do
319 Norte. The coast is very irregular in plan-view, being characterized by several embayments and
320 promontories, with steep cliffs carved in the eastward-prograding lava-delta sequences of the Pico
321 Alto Volcanic Complex (Fig. 2). The NNW-SSE oriented shelf runs parallel to the coastline and is c.
322 0.6-2.4 km wide, being wider offshore Ponta do Castelete and São Lourenço bay (Figs 8a and 8b).
323 The erosive shelf edge depth varies mostly between 80 m and 100 m between Ponta do Norte and
324 the shelf edge embayment offshore Pontinha, whilst south of Potinha it is much shallower, being
325 between 50 m and 100 m (Figs. 8a and 8b). Rocky outcrops are frequently extended down to the
326 shelf edge, where in places they form eastward-dipping ramps, with landward lips up to few
327 meters high (Fig. 8a and seismic profile hh' in Fig. 8ESM). Apart from some small-scale
328 indentations affecting the shelf edge, the eastern sector exhibits only an evident embayment that
329 dissects the shelf at c. -60- -80 m offshore Pontinha, in front of a concave cliff on the coast (Fig.
330 8a).
331 The distribution between the sedimentary cover and rocky surfaces is very similar to the
332 northern and southern sectors, with 54% corresponding to sediments and 46% corresponding to
333 rocky surfaces. This sector has a total of 0.187 km^3 of sediments and a ratio volume of
334 sediments/shelf surface area of 0.015. Along the eastern shelf sector the sediments fill some
335 depressions bordered by rocky outcrops and cover the shelf down to c. -70 m, showing a thickness

336 variable from 2 to 15 m (Fig. 9). The most extensive sediment accumulation, lying offshore
337 Pontinha is a depression between rocky outcrops (Figs. 9 and 9ESM).
338
339 ## *4.2 Wave regime around Santa Maria Island*
340 The ERA outputs of Santa Maria wave properties suggest that the prevailing swells approach
341 Santa Maria Island from the northwest (35%) and west (22%), with average significant wave
342 heights (H_s) of 2.14 m and 2.44 m respectively (Fig. 10 and Table 1). Waves from north and
343 northeast are also frequent (respectively 19% and 12%) but lower (respectively H_s of 1.92 m and
344 1.83 m). The remaining directions are insignificant (< 5% each), however waves from the
345 southwest can still reach 2.45 m, but only during 5% of the year.
346
347 # *5. Discussion*
348
349 ### *5.1 Sediment distribution on the shelf*
350 In principle the shelf sectors surrounding the eastern part of Santa Maria should be filled with
351 more sediment because cliffs are higher and streams are more abundant. In what concerns
352 accommodation space the western, southern and eastern shelf sectors have similar areas, hence
353 similar space to accommodate deposits (see Table 1). However, the western shelf is mostly
354 sediment-free, with deposits only on the outer shelf and very thin (c. 2 m thick, Fig. 9). The ratio
355 volume of sediments to area of the shelf in this sector is the lowest (0.003) and around one quart
356 to one fifth of the southern and eastern sectors (respectively 0.012 and 0.015) The southern and
357 eastern shelf sectors exhibit then a wider sedimentary cover (around 50% of the seafloor), but
358 mostly located in the middle to outer shelf. The northern sector shows a similar sediment
359 distribution pattern to the southern and eastern sectors, although being much wider. The deposits

are very thin (c. 2m) and are mostly on the middle to outer shelf. The fact that nearshore areas of the four sectors are mostly sediment-stripped, despite that most sediments should be produced from cliff erosion is somehow puzzling. This sediment distribution pattern is also seen in other islands of the Azores archipelago such as Faial and Pico and related with high wave energy of this archipelago (Quartau et al., 2012; Quartau et al., 2015b). At Santa Maria this pattern is exacerbated on the western sector relatively to the southern and eastern sectors because this sector is more exposed to the dominant waves, hence transport of sandy sediments to deeper areas is higher and these are probably lost to the slope. In addition, this sector has a poorly developed subaerial drainage and the cliffs are smaller, so fewer sediments accumulate nearshore. Sediments of the southern and eastern shelf sectors, being on the leeward side of the island are less easily transported offshore and consequently may rest at shallower depths (from 35/40 m downwards). The presence of preserved small terraces and wave-cut notches attributed to the last interglacial (and older interglacials) along the SE, E and NE shores (Ramalho et al., 2017) also suggests that wave influence is also lower in these sectors, otherwise these morphologies would have been obliterated receding cliff erosion. In addition, these sectors are partially or entirely adjacent to the higher and rainier side of the island, with a more evolved subaerial drainage, which presumably delivers higher quantities of sediments that then accumulate nearshore. The northern sector is also exposed to the dominant waves as the western sector. However, given that this sector is much wider, sediments are probably not transported much further than the middle to outer shelf and thus are not entirely lost to the slope, leading to a higher sediment accumulation when compared with the western sector. Nevertheless, due to such a large accommodation space, the ratio volume of sediments to area of the shelf in this sector is still the second lowest (0.014) after the western sector.

383 The shelf around Santa Maria lacks well-developed sedimentary bodies as those recognized on
384 other islands of the Azores and the Mediterranean Sea where some portions of the shelf are
385 covered by up to 30-40 m thick volcaniclastic sequences (Chiocci and Romagnoli, 2004; Quartau et
386 al., 2012; Casalbore et al., 2017; Romagnoli et al., 2020). Given that Santa Maria is much older and
387 eroded for a longer period of time should not the shelf have thicker deposits? We believe that the
388 thin sediment cover offshore Santa Maria can be explained by three main reasons:
389
390 1. Increasing wave attenuation with shelf width. As shelves became wider, not only the space
391 for sediment accommodation increases, but the energy reaching the coastline decreases
392 due to wave attenuation over wider and shallower shelves (Quartau et al., 2010).
393 Consequently, the lower sediment production by cliff retreat and the higher
394 accommodation space explains the thin cover around Santa Maria shelf.
395 2. Santa Maria Island is a low and small island, with less precipitation and lower rates of
396 stream erosion when compared with other Azorean Islands (which exhibit rainfall regimes
397 frequently above 2000 mm/year, AEM & IMP, 2012). Thus, sediment production is likely
398 dominated by cliff erosion. On the other hand given that island is mostly bound by low cliffs,
399 their erosion produces less sediments than in taller islands.
400 3. Preservation issues, i.e., the weaker potential for preservation of depositional sequences on
401 the shelves of reefless volcanic islands that are subjected to highly-energetic wave regimes.
402 The Azores archipelago is considered an energetic environment in terms of winds and wave
403 action (Andrade et al., 2008; Quartau et al., 2012; Rusu and Guedes Soares, 2012). In these
404 settings, sediments tend to be transported offshore. Furthermore, as sea level falls, most of
405 the sediments are transported below the shelf edge, leaving the shelves completely
406 stripped of sediments. This cycle is repeated every glacio-eustatic oscillation, preventing the

accumulation of several depositional sequences, as seen on continental shelves (Ávila et al, 2008; Quartau et al., 2012).

The preservation issues also apply to other volcanic ocean islands subjected to high wave energy regimes. However, on the case of Santa Maria, the two previous reasons are more relevant and probably are enough to explain why Santa Maria lacks thicker sedimentary deposits in its shelf.

5.2 Mass wasting processes

Hampton et al. (1996) and Locat and Lee (2002) suggested several mechanisms for submarine landslide triggering. These may include oversteepening, seismic and storm-wave loading and the incohesive nature of the sediments. The subaerial and submarine flanks of volcanic islands are prone to be affected by large-scale sector collapses, as attested by both collapse scars and submarine deposits seen in archipelagos such as the Hawaii (Moore et al., 1994), Canaries (Masson et al., 2002), Cape Verde (Masson et al., 2008), Aeolian (Romagnoli et al., 2009a; Romagnoli et al., 2009b), Aleutians (Montanaro and Beget, 2011), Azores (Costa et al., 2015; Quartau et al., 2015b) and Madeira (Quartau et al., 2018a). Large-scale flank collapses have been proposed for Santa Maria by Sibrant et al. (2015) but at least the younger collapse proposed by these authors is at odds with onshore field studies documented by Ramalho et al. (2017), and submarine evidence for these collapses is absent. However, small scale mass wasting features were identified at the edge of the insular shelf surrounding Santa Maria Island, and these are mostly concentrated on the northern and southern sectors. The largest scars are located along the NE shelf edge, between the areas offshore Ponta do Norte and Baía da Cré, and exhibit a wide

431 semicircular shape (Fig. 5a). Several gully heads, with an elongated shape, are also found at the
432 southern shelf edge, between the areas offshore Vila do Porto and Praia Formosa (Fig. 7a). These
433 morphological differences might be related to the processes responsible for the formations of the
434 scars. Along the edge of the NE shelf sector, the scars are apparently controlled by the distribution
435 of the eroded cones and the rocky outcrops on the shelf (Fig. 5a). The areas between the
436 cones/outcrops are probably composed of more friable materials, thus representing a possible
437 lithological weakness, and a preferential pathway for sediment reworking. Despite the fact that
438 nowadays the wide northern shelf prevents any direct stream discharge onto the outer shelf and
439 the upper submarine slope beyond the shelf break, during lowstands sedimentary flows probably
440 were able to reach these areas, carving the head of those "proto-gullies".

441 Cones are absent along the southern shelf sector, where the elongated morphology of the scars
442 seem to reflect instead NE-SW striking structural weakness corridors, related to the faults that
443 extend to the south of the island and affect the shelf inducing localized erosion (Fig. 7a). The same
444 structural control might be inferred for the formation of the narrow scar located at the shelf edge
445 offshore Ponta dos Frades, in the northern shelf sector (Fig. 5a), being probably the continuation
446 of the faults recognized onshore (Madeira et al., 2015) and on the inner part of the shelf (Ricchi et
447 al., 2018). Similar features can be found on the NE, southern and eastern shelf sectors where likely
448 fault-controlled basins coincide with the scars of shelf-edge landslide (Fig. 9 and profile b-b´ in Fig.
449 3ESM, profile f-f' in Fig. 6ESM and profile i-i' in Fig. 9ESM).

450 In the case of Santa Maria, it appears that on the southern and in some places on the eastern
451 shelves and northern shelf these mass-wasting processes are mostly controlled by tectonics,
452 because scars appear to be the extension of onshore tectonic features. However, on the northern
453 shelf sector, tectonics appears to play a smaller role. On these sites it is more likely that the
454 accumulation of incohesive sediments near the shelf edge (with high gradients) might trigger

455 those landslides as suggested by Casalbore et al. (2015) in Terceira Island, Quartau et al. (2012) in
456 Faial Island, Quartau et al. (2018a) and Santos et al. (2019) in Madeira archipelago, promoting
457 shelf edge retreat. A quite similar setting is found in other shelves around Italian islands, such as
458 Vulcano (Romagnoli et al., 2013), Lipari (Casalbore et al., 2016a), and Ventotene islands (Casalbore
459 et al., 2016b), evidencing how the shelf edge is susceptible to landsliding processes. Most of these
460 islands are volcanic active, thus the production of volcanogenic sediment is higher favoring the
461 widespread occurrence of small-scale mass wasting, especially where thick volcanogenic aprons
462 are present. On the western side of Santa Maria, probably due to the scarcity of sediments and
463 faults there are no significant scars at the shelf edge.
464
465 ***5.3 New insights on the evolution of Santa Maria Island from submarine morphologies***
466
467 Here we discuss the evolution of Santa Maria Island, based on the analysis of the morphologic
468 parameters of the shelf (erosive shelf edge depth, shelf width, and type of submarine
469 morphologies, Figures 5-8 and Table 1).
470
471 ***5.3.1 Insights from the shelf width***
472 Generally, on volcanic islands a correspondence between shelf width and age of volcanic
473 products outcropping onland is found (Menard, 1983). The width/age relationship is associated to
474 the fact that the shelf width increases with increasing time as shorelines retreat with prolonged
475 exposure to marine erosion (Quartau et al., 2010, 2012, 2014; Romagnoli, 2013; Romagnoli et al.,
476 2018).
477 At Santa Maria this relationship can be better observed between the two width/age extremes,
478 the northern shelf (up to c. 8.7 km), likely carved in the c. 5.8 Ma-old Anjos volcanic products, and

479 the eastern shelf (2.4 km), carved in the c. 4.1-3.5 Ma old products of the Pico Alto volcanic
480 Complex (Figs. 2 and 4). However, the western shelf shows a dramatically lower width (up to c. 2.3
481 km) with respect the northern one (up to c. 8.7 km), despite both sectors are carved in the Anjos
482 volcanic products and are similarly exposed to the same dominant waves. Remarkably, the
483 western sector shelf is generally narrower than the southern one (2.6 km, also carved in the Anjos
484 volcanic units) and with similar width to the eastern sector (2.4 km). This apparent incongruence
485 can be explained by the paleogeography of the island in its earlier stages of growth. The western
486 subaerial side of the island is interpreted as an uplifted shelf that, at the onset of the uplift (3.5
487 Ma), was entirely submerged (Fig. 11) as suggested by presently exposed subaerial marine
488 terraces (Ramalho et al., 2017; Ricchi et al., 2018). The width of the western shelf, if measured
489 from the paleo-coastline attributed to 3.5 Ma BP is between 5.3 km and 8.5 km (Fig. 11). This
490 explains why the western shelf, today is not wider than the leeward and younger southeastern
491 and eastern shelves. However, it does not explain why the northern is presently much wider than
492 the western shelf. Given that both northern and western shelves are exposed to similar wave
493 energy they should have similar widths (Figs. 5 and 6 and Table 1ESM).
494
495 ***5.3.2 Insights from the shelf edge depth***
496 The analysis of the shelf edge depth might also help us in our understanding (Figs. 5-8). The
497 erosive shelf edge depth is related to sea level coeval to the shelf formation; therefore this
498 morphological feature can be used as a marker of palaeo sea levels, and thus be used to assess
499 subsequent vertical movements affecting the volcanic edifices (Quartau et al. 2014; 2016,
500 Romagnoli et al., 2018, Lucchi et al., 2019). Since glacial eustatic sea level never reached depths
501 below 125 m in the last 3.5 Ma (Bintanja and van de Wal, 2008; de Boer et al., 2010), so any part
502 of the shelf that is presently located below this depth should have experienced net subsidence

(Quartau et al., 2014; Quartau et al., 2015b; 2016; Quartau et al., 2018b; Romagnoli et al., 2018). Given that Santa Maria was affected by early subsidence prior to a reversal into an uplift trend at ~3.5 Ma (Ramalho et al., 2017), the portions of the shelf exhibiting the deepest erosive edges can be considered the oldest since they underwent the largest submergence after formation. According to the history of vertical movements reconstructed for Santa Maria (Ramalho et al., 2017; Ricchi et al., 2018), the northern shelf sector, being the deepest of all (erosive shelf edge depth down to -170 m, Figs. 5a and 5b), can be thus considered the oldest in formation. Deep (>-125 m) shelf edges have been also identified offshore the western sector of the island. However, in this shelf sector the maximum edge depth is 154 m (Figs. 5 and 6), indicating that it has suffered less subsidence than the northern shelf. Being likely carved in the products of the Anjos Volcanic Complex (Fig. 2) this shelf sector might be younger than the northern portion of the shelf.

Along the southern shelf sector, the shelf exhibits a more complex morphology and the shelf edge depth has a strongly irregular trend mostly around 80/100 m and being locally at 50/60 m (Fig. 7). The deeper shelf edge offshore Ponta do Castelo (147 m) is in agreement with the inferred subsidence processes experienced by the island and the relatively old age of this shelf sector. It is comparable to the maximum depth along the western sector (154 m, Fig. 6), suggesting that the southeastern portion of Santa Maria could be as old as the western portion of the island if they had been exposed to the same vertical movements.

The eastern shelf shows shelf edge depths not deeper than 100 m, contrary to the remaining sectors that show depths below 125 m. This is because when Pico Alto volcanism ended, the island was on a turning point in terms of vertical movements (see Fig. 6 of Ramalho et al., 2017). It was the beginning of the uplift trend, so the erosional shelf edge of this sector never experienced subsidence and is now always well above 125 m.

5.3.3 Insights from submarine morphologies

5.3.3.1 Northern shelf sector

The morphology of the NW inner shelf shows, from Baía do Mar da Barca to Baía da Cré, a ~3 km wide belt of flat rocky outcrops that is very similar to those that can be seen on the western shelf (Figs. 5a and 6a). This suggests that, most likely, this area was carved on the Anjos Volcanic Complex. We believe that an earlier part of the island, probably older than the products of the Anjos Volcanic Complex, lies offshore those rocky outcrops on the northern shelf. This limit cannot be followed eastwards due to the profusion of eroded prominent reliefs existing in this portion of the shelf.

From Baía da Cré to the east, all rocky features are interpreted as volcanic cones or other type of eruptive centers, albeit being of different age and having experienced different degrees and styles of differential erosion. Type (a) described in section 4.1.1 are interpreted either as volcanic necks exposed by differential erosion, or also as pillow mounds. Type (b), with their concentric nature, are interpreted as old, well-consolidated strombolian cinder-and-scoria cones exposed and truncated by marine erosion. It is unlikely these are recent surtseyan cones, given that surtseyan cones are more friable and typically erode to a flat platform (notwithstanding some concentric features), as the recent surveys of Surtla, Jólnir and Syrtlingur (Surtsey, Iceland; see Romagnoli & Jacobson, 2015) suggest. These cones are probably contemporary of either the Porto Formation or the Anjos Volcanic Sequence, given their inferred subaerial nature and the fact that the only time relative sea level was low enough to allow their formation was during the period between 5.8 and 5.3 Ma (see Figs. 6 and 7 of Ramalho et al. 2017). In a similar fashion, type (c) cones are interpreted as subaerial cones buried by effusive sequences, which are more erosion-resistant than the softer inner core of the cinder cones. Given this, and the fact that these cones were buried by effusive sequences that are in continuity with the Anjos Volcanic sequence onshore, and

551 given that they do not exhibit any of the prominent concentric morphologies typical of type (b)
552 cones, these morphologies are interpreted to correspond to eroded surtseyan cones of the
553 Cabrestantes Formation. Finally, type (d) cones, given their very pristine ring-like morphologies,
554 with very low degrees of erosion, are interpreted as very young volcanic cones, perhaps younger
555 than any structure found onshore.

556 The NNW-SSE submarine rocky ridge (Fig. 5a) that extends offshore Ilhéu das Lagoínhas is in
557 clear alignment with both the dykes that cross-cut the Anjos Volcanic Complex along the adjacent
558 coastline and the Pico Alto's ridge. This suggests long-lived fissural volcanism roughly oriented N-S
559 in this part of the island, both during the Anjos and Pico Alto's volcanic phases. This inference is
560 also supported by the presence of elongated morphologies interpreted as dykes exposed by
561 differential erosion (Figs. 4 and 1ESM).

562 The pillow-lava cone of Baixa do Ambrósio at the NW edge of the northern shelf (Fig. 5a) is not
563 directly associated to any of the volcanic complexes making up Santa Maria Island. The lack of
564 dated samples prevented us to make any inference regarding its earlier growth. The depth of its
565 top (c. 50 m) suggests that probably it is younger with respect the rest of the northern shelf
566 sector; otherwise it would be a more flat-topped cone. On its flanks, Ricchi et al. (2018) recognized
567 a set of submerged marine terraces from 70/80 m to 120/140 m. The shallowest terraces are
568 considered to be the oldest and were likely carved at least since 866 ka (Ricchi et al., 2018),
569 suggesting that the cone is older than this age.

570 We therefore infer that all these eroded cones are covering a "proto-Santa Maria Island" on
571 which the outer northern shelf was carved. This shelf is much wider than the western shelf and the
572 shelf edge deeper. The occurrence of an older volcanic edifice offshore the northern portion of the
573 island had already been proposed by Ramalho et al. (2017), based on the wide northern shelf. But

574 now, an improved insight can be taken from the interpretation of the deeper shelf edge and high-
575 resolution images of the submarine morphologies.
576
577 5.3.3.2 Western shelf sector
578 The morphology of this sector shows a ~1-2 km wide belt of flat rocky outcrops that is very
579 similar to those that can be seen on the NW inner shelf (Figs. 5a and 6a). This suggests that, most
580 likely, this area was carved on Anjos Volcanic Complex.
581
582 5.3.3.3 Southern shelf sector
583 This shelf sector shows a ~0.7-2.3 km wide belt of flat rocky outcrops (Fig. 7a) that are very
584 similar to those on the NW inner shelf and western shelf (Figs. 5a and 6a). These rocky outcrops
585 are separated by sedimentary bottoms that correspond to fault controlled basins. The similarity
586 with the NW inner shelf and western shelf suggests that, most likely, this area was also carved on
587 Anjos Volcanic Complex.
588
589 5.3.3.4 Eastern shelf sector
590 The association of the eastern shelf sector to the Pico Alto products is supported by the outer
591 shelf morphology, which fin-like outward dipping rocky surfaces (Fig. 8 and seismic profile hh' in
592 Fig. 8ESM), interpreted as preserved substructural surfaces of the foreset units of Gilbert-type
593 lava-fed deltas. Effectively, these morphologies are in structural continuity with the eastward-
594 dipping foreset units of the lava-fed delta sequences that crop out all along the eastern coast of
595 the island (e.g. see Figs. 3G and 3H of Ramalho et al. 2017), which extend from the passage zone
596 (between subaerial topset and submarine foreset units) currently located up to c. 130 m in
597 elevation to present-day sea level (Ramalho et al., 2017). These observations therefore suggest

598 that the eastern submarine upper slope of Santa Maria corresponds to the outer submarine slopes
599 of former Gilbert-type lava-fed deltas, i.e. are constructional morphologies contemporaneous of
600 the eastward expansion of the Pico Alto volcanic edifice, prior to uplift and erosion of the shelf.
601
602 ## *6. Conclusions*
603
604 The morphologic analysis of the shelf surrounding Santa Maria Island complemented with the
605 known geological history of the subaerial island allowed us to improve our understanding of the
606 island's evolution and the processes which have shaped its shallow submerged portions.
607 The shelves surrounding Santa Maria are mostly sediment-starved. Around 50% of the shelf is
608 rocky and sediment thickness is on average less than 2 m. A few depocenters exist, however, with
609 thicknesses up to 14 m, but these are clearly fault-controlled basins. The lack of thicker and older
610 submarine deposits that should have accumulated by erosion of the subaerial flanks of the island
611 are related with the high wave energy in the Azores and the cyclicity of sea-level changes. High
612 wave energy tends to transport sediments offshore and during sea level falls, sediments that
613 normally accumulate on the shelf are swept offshore until they are lost to the slopes as they cross
614 the shelf edge. In the present-day, and since shelves are wide, waves tend to attenuate their
615 energy, eroding the cliffs with less efficiency. In addition, it has lower cliffs and rains less, when
616 compared to other studied islands, so fewer sediments are expected to be delivered from the
617 island to the coastline. Thus, not only fewer sediments are produced, but also larger
618 accommodation spaces (wider shelves) preclude the existence of thicker submarine deposits, as
619 found on other studied volcanic islands.
620 Small mass-wasting features were found on the shelf edge of Santa Maria. These are mostly
621 restricted to the northern and southern shelves, with only one evident scar on the eastern shelf.

622 However, different processes appear to be responsible for such features. On the southern and
623 eastern shelf sectors, is mostly tectonics that controls the location of mass-wasting morphologies,
624 with faults extending offshore and reaching the shelf break. On the northern shelf, the
625 predisposing factor is mostly the accumulation of unconsolidated sediments near the edge.
626 Based on the analysis of the shelf geomorphic features (shelf width, erosive shelf edge depth
627 and morphology) and the correlation with volcanic sequences outcropping on the island, we were
628 able to improve our understanding of Santa Maria geological evolution. We suggest that given the
629 wide extension of the northern shelf, its outer part belongs to an older and undated volcanic
630 sequence of Santa Maria that predated the Cabrestantes and Porto Formations. The mid-to inner
631 northern shelf, as well as the western and southern shelves were probably carved mainly on the
632 products of Anjos Volcanic Complex, whilst the eastern shelf results from erosion of the products
633 of Pico Alto Volcanic Complex. The present-day narrow width of the western shelf, when
634 compared with the southern and eastern shelves, which are more protected to wave erosion, can
635 be explained by the uplift mechanism that raised part of the western shelf, originally ~5.3-8.5 km
636 wide, leaving now a ~2 km wide shelf.
637 This work shows that, despite the fact that Santa Maria Island is much older than islands
638 addressed in previous shelf studies, the various geological processes acting on the shelf can still
639 leave significant morphological imprints that provide us important knowledge about the
640 evolutionary history of this island.
641

642 ## *7. Acknowledgments*

643 The acquisition of multibeam bathymetry and seismic reflection profiles were funded by Fundação
644 para a Ciência e a Tecnologia (FCT) through the PLATMAR project (*Development of volcanic island*
645 *shelves: insights from Sta. Maria Island and implications on hazard assessment, habitat mapping*

646 *and marine aggregates management,* PTDC/GEO-GEO/0051/2014). The authors are grateful to the
647 crew of R/V Arquipélago and Pedro Afonso for all their help in the preparation and execution of
648 the geophysical survey. R. Ramalho acknowledges its “Investigador FCT” contract IF/01641/2015
649 funded by FCT. This study has been developed in the framework of the PhD thesis “Insular shelves
650 as a tool for reconstructing the evolution of volcanic islands” (A. Ricchi, University of Bologna).
651

652 ## *8. References*

653

654 Agencia Estatal de Meteorología & Instituto de Meteorologia de Portugal, 2012. Climate atlas of
655 the archipelagos of the Canary Islands, Madeira and the Azores. p. 78.

656 Andrade, C., Trigo, R.M., Freitas, M.C., Gallego, M.C., Borges, P., Ramos, A.M., 2008. Comparing
657 historic records of storm frequency and the North Atlantic Oscillation (NAO) chronology for the
658 Azores region. The Holocene 18, 745-754.

659 Ávila, S.P., Madeira, P., Silva, C.M.d., Cachão, M., Quartau, R., Landau, B., Martins, A.M.d.F., 2008.
660 Local disappearance of bivalves in the Azores during the last glaciation. Journal of Quaternary
661 Science 23, 777-785.

662 Bintanja, R., van de Wal, R.S.W., 2008. North American ice-sheet dynamics and the onset of
663 100,000-year glacial cycles. Nature 454, 869-872.

664 Casalbore, D., Bosman, A., Romagnoli, C., Di Filippo, M., & Chiocci, F.L., 2016a. Morphology of
665 Lipari offshore (Southern Tyrrhenian Sea). Journal of Maps 12, 77-86.

666 Casalbore, D., Bosman, A., Martorelli, E., Sposato, A., Chiocci, F.L., 2016b. Mass wasting features
667 on the submarine flanks of Ventotene volcanic edifice (Tyrrhenian Sea, Italy): In Submarine Mass

668 Movements and Their Consequences, (Eds Krastel et al), Advances in Natural and Technological
669 Hazards Research, 37, 285-293, DOI 101007/978-3-319-00972-8 25

670 Casalbore, D., Falese, F., Martorelli, E., Romagnoli, C., Chiocci, F.L., 2017. Submarine depositional
671 terraces in the Tyrrhenian Sea as a proxy for paleo-sea level reconstruction: Problems and
672 perspective. Quatern. Int. 439, 169-180.

673 Casalbore, D., Romagnoli, C., Adami, C., Bosman, A., Falese, F., Ricchi, A., Chiocci, F., 2018.
674 Submarine Depositional Terraces at Salina Island (Southern Tyrrhenian Sea) and Implications on
675 the Late-Quaternary Evolution of the Insular Shelf. Geosciences 8, 20.

676 Casalbore, D., Romagnoli, C., Bosman, A., Chiocci, F.L., 2011. Potential tsunamigenic landslides at
677 Stromboli Volcano (Italy): Insight from marine DEM analysis. Geomorphology 126, 42-50.

678 Casalbore, D., Romagnoli, C., Pimentel, A., Quartau, R., Casas, D., Ercilla, G., Hipólito, A., Sposato,
679 A., Chiocci, F.L., 2015. Volcanic, tectonic and mass-wasting processes offshore Terceira Island
680 (Azores) revealed by high-resolution seafloor mapping. Bull. Volc. 77, 1-19.

681 Chiocci, F.L., Romagnoli, C., 2004. Submerged depositional terraces in the Aeolian Islands (Sicily),
682 in: Chiocci, F.L., D'Angelo, S., Romagnoli, C. (Eds.), Atlas of submerged depositional terraces along
683 the Italian coasts. Memorie Descrittive della Carta Geologica d'Italia. APAT, Roma, pp. 81-114.

684 Costa, A.C.G., Hildenbrand, A., Marques, F.O., Sibrant, A.L.R., Santos de Campos, A., 2015.
685 Catastrophic flank collapses and slumping in Pico Island during the last 130 kyr (Pico-Faial ridge,
686 Azores Triple Junction). J. Volcanol. Geotherm. Res. 302, 33-46.

687 de Boer, B., Van De Wal, R.S.W., Bintanja, R., Lourens, L.J., Tuenter, E., 2010. Cenozoic global ice-
688 volume and temperature simulations with 1-D ice-sheet models forced by benthic 18O records.
689 Ann. Glaciol. 51, 23-33.

690 Dee, D. P., S. Uppala, A. Simmons, P. Berrisford, P. Poli, S. Kobayashi, U. Andrae, M. Balmaseda, G.
691 Balsamo, and P. Bauer., 2011. The ERA-Interim reanalysis: Configuration and performance of the
692 data assimilation system. Q. J. Roy. Meteor. Soc., 137 (656), 553-597.

693 Deplus, C., Le Friant, A., Boudon, G., Komorowski, J.-C., Villemant, B., Harford, C.L., Segoufin, J.,
694 Cheminée, J.-L., 2001. Submarine evidence for large-scale debris avalanches in the Lesser Antilles
695 Arc. Earth Planet. Sci. Lett. 192, 145-157.

696 Fernandes, J., 2004. Caracterização Climática das ilhas de S Miguel e Santa Maria com base no
697 modelo CIELO. BSc thesis. Dept. de Ciências Agrárias. Universidade dos Açores, Angra do
698 Heroísmo, p. 210.

699 Field, M.E., Roy, P.S., 1984. Offshore transport and sand-body formation; evidence from a steep,
700 high energy shoreface, southeastern Australia. J. Sediment. Res. 54, 1292-1302.

701 Gente, P., Dyment, J., Maia, M., Goslin, J., 2003. Interaction between the Mid-Atlantic Ridge and
702 the Azores hot spot during the last 85 Myr: Emplacement and rifting of the hot spot-derived
703 plateaus. Geochem. Geophys. Geosyst. 4, 8514.

704 Hampton, M.A., Lee, H.J., Locat, J., 1996. Submarine landslides. Rev. Geophys. 34, 33-59.

705 Hatton, B. 2019. Hurricane Lorenzo batters mid-Atlantic Azores Islands. ABC News. Associated
706 Press. Retrieved February 9, 2020.

URL:https://abcnews.go.com/International/wireStory/category-hurricane-batters-mid-atlantic-azores-islands-65997843.

Hernández-Molina, F.J., Fernández-Salas, L.M., Lobo, F., Somoza, L., Díaz-del-Río, V., Alveirinho Dias, J.M., 2000. The infralittoral prograding wedge: a new large-scale progradational sedimentary body in shallow marine environments. Geo-Mar. Lett. 20, 109-117.

Hipólito, A., Madeira, J., Carmo, R., Gaspar, J.L., 2013. Neotectonics of Graciosa island (Azores): a contribution to seismic hazard assessment of a volcanic area in a complex geodynamic setting. Ann. Geophys. 56, 1-18.

Krastel, S., Schmincke, H.-U., Jacobs, C.L., 2001. Formation of submarine canyons on the flanks of the Canary Islands. Geo-Mar. Lett. 20, 160-167.

Lebas, E., Friant, A.L., Deplus, C., Voogd, B., 2018. Understanding the Evolution of an Oceanic Intraplate Volcano From Seismic Reflection Data: A New Model for La Réunion, Indian Ocean. J. Geophys. Res. Solid Earth 123, 1035-1059.

Llanes, P., Herrera, R., Gómez, M., Muñoz, A., Acosta, J., Uchupi, E., Smith, D., 2009. Geological evolution of the volcanic island La Gomera, Canary Islands, from analysis of its geomorphology. Mar. Geol. 264, 123-139.

Locat, J., Lee, H.J., 2002. Submarine landslides: advances and challenges. Can. Geotech. J. 39, 193-212.

Lourenço, N., Miranda, J.M., Luís, J.F., Ribeiro, A., Mendes Victor, L.A., Madeira, J., Needham, H.D., 1998. Morpho-tectonic analysis of the Azores Volcanic Plateau from a new bathymetric compilation of the area. Mar. Geophys. Res. 20, 141-156.

728 Lucchi, F., Ricchi, A., Romagnoli, C., Casalbore, D., Quartau, R., 2019. Late Quaternary paleo sea
729 level geomorphological markers of opposite vertical movements at Salina volcanic island (Aeolian
730 Arc). Earth Surf. Proc. Land., , https://doi.org/10.1002/esp.4651. .

731 Madeira, J., 1986. Geologia estrutural e enquadramento geotectónico da ilha de Santa Maria, MSc
732 thesis. Dept. de Geologia. Universidade de Lisboa, Lisboa, p. 107.

733 Madeira, J., Brum da Silveira, A., Hipólito, A., Carmo, R., 2015. Active tectonics in the central and
734 eastern Azores islands along the Eurasia–Nubia boundary: a review, in: Gaspar, J.L., Guest, J.E.,
735 Duncan, A.M., Barriga, F.J.A.S., Chester, D.K. (Eds.), Geological Society, London, Memoirs, 44, pp.
736 15-32.

737 Marques, F.O., Catalão, J.C., DeMets, C., Costa, A.C.G., Hildenbrand, A., 2013. GPS and tectonic
738 evidence for a diffuse plate boundary at the Azores Triple Junction. Earth Planet. Sci. Lett. 381,
739 177-187.

740 Masson, D.G., Le Bas, T.P., Grevemeyer, I., Weinrebe, W., 2008. Flank collapse and large-scale
741 landsliding in the Cape Verde Islands, off West Africa. Geochem. Geophys. Geosyst. 9,
742 doi:10.1029/2008GC001983.

743 Masson, D.G., Watts, A.B., Gee, M.J.R., Urgeles, R., Mitchell, N.C., Le Bas, T.P., Canals, M., 2002.
744 Slope failures on the flanks of the western Canary Islands. Earth-Sci. Rev. 57, 1-35.

745 Mazuel, A., Sisavath, E., Babonneau, N., Jorry, S.J., Bachèlery, P., Delacourt, C., 2016. Turbidity
746 current activity along the flanks of a volcanic edifice: The Mafate volcaniclastic complex, La
747 Réunion Island, Indian Ocean. Sed. Geol. 335, 34-50.

748 Meireles, R., Quartau, R., Ramalho, R.S., Rebelo, A.C., Madeira, J., Zanon, V., Ávila, S.P., 2013.
749 Depositional processes on oceanic island shelves – evidence from storm-generated Neogene
750 deposits from the mid-North Atlantic. Sedimentology 60, 1769-1785.

751 Menard, H.W., 1983. Insular erosion, isostasy, and subsidence. Science 220, 913-918.

752 Miranda, J.M., Luís, J., Lourenço, N., 2018. The geophysical architecture of the Azores from
753 magnetic data, in: Kueppers, U., Beier, C. (Eds.), Volcanoes of the Azores. Springer-Verlag Berlin
754 Heidelberg, pp. 89-100.

755 Mitchell, N.C., Dade, W.B., Masson, D.G., 2003. Erosion of the submarine flanks of the Canary
756 Islands. J. Geophys. Res. 108, 3-1 - 3-11.

757 Mitchell, N.C., Masson, D.G., Watts, A.B., Gee, M.J.R., Urgeles, R., 2002. The morphology of the
758 flanks of volcanic ocean islands: A comparative study of the Canary and Hawaiian hotspot islands.
759 J. Volcanol. Geotherm. Res. 115, 83-107.

760 Montanaro, C., Beget, J., 2011. Volcano collapse along the Aleutian Ridge (western Aleutian Arc).
761 Nat. Hazards Earth Syst. Sci. 11, 715-730.

762 Moore, J.G., Clague, D.A., Holcomb, R.T., Lipman, P.W., Normark, W.R., Torresan, M.E., 1989.
763 Prodigious submarine landslides on the Hawaiian Ridge. J. Geophys. Res.: Solid Earth 94, 17465-
764 17484.

765 Moore, J.G., Normark, W.R., Holcomb, R.T., 1994. Giant Hawaiian Landslides. Annu. Rev. Earth Pl.
766 Sc. 22, 119-144.

767 Oehler, J.-F., Lénat, J.-F., Labazuy, P., 2008. Growth and collapse of the Reunion Island volcanoes.
768 Bull. Volc. 70, 717-742.

769 Quartau, R., Hipólito, A., Mitchell, N.C., Gaspar, J.L., Brandão, F., 2015a. Comment on
770 “Construction and destruction of a volcanic island developed inside an oceanic rift: Graciosa
771 Island, Terceira Rift, Azores” by Sibrant et al. (2014) and proposal of a new model for Graciosa
772 geological evolution [J. Volcanol. Geotherm. Res. 284 (2014) 32-45]. J. Volcanol. Geotherm. Res.
773 303, 146-156.

774 Quartau, R., Hipólito, A., Romagnoli, C., Casalbore, D., Madeira, J., Tempera, F., Roque, C., Chiocci,
775 F.L., 2014. The morphology of insular shelves as a key for understanding the geological evolution
776 of volcanic islands: Insights from Terceira Island (Azores). Geochem. Geophys. Geosyst. 15, 1801–
777 1826.

778 Quartau, R., Madeira, J., Mitchell, N.C., Tempera, F., Silva, P.F., Brandão, F., 2015b. The insular
779 shelves of the Faial-Pico Ridge: a morphological record of its geologic evolution (Azores
780 archipelago). Geochem. Geophys. Geosyst. 16, 1401–1420.

781 Quartau, R., Madeira, J., Mitchell, N.C., Tempera, F., Silva, P.F., Brandão, F., 2016. Reply to
782 comment by Marques et al. on “The insular shelves of the Faial-Pico Ridge (Azores archipelago): A
783 morphological record of its evolution”. Geochem. Geophys. Geosyst. 17, 633-641.

784 Quartau, R., Mitchell, N.C., 2013. Comment on "Reconstructing the architectural evolution of
785 volcanic islands from combined K/Ar, morphologic, tectonic, and magnetic data: The Faial Island
786 example (Azores)" by Hildenbrand et al. (2012) [J. Volcanol. Geotherm. Res. 241-242 (2012) 39-
787 48]. J. Volcanol. Geotherm. Res. 255, 124-126.

788 Quartau, R., Ramalho, R.S., Madeira, J., Santos, R., Rodrigues, A., Roque, C., Carrara, G., Brum da
789 Silveira, A., 2018a. Gravitational, erosional and depositional processes on volcanic ocean islands:

790 Insights from the submarine morphology of Madeira archipelago. Earth Planet. Sci. Lett. 482, 288-
791 299.

792 Quartau, R., Tempera, F., Mitchell, N.C., Pinheiro, L.M., Duarte, H., Brito, P.O., Bates, R., Monteiro,
793 J.H., 2012. Morphology of the Faial Island shelf (Azores): The interplay between volcanic,
794 erosional, depositional, tectonic and mass-wasting processes. Geochem. Geophys. Geosyst., 13,
795 Q04012, doi:10.1029/2011GC003987.

796 Quartau, R., Trenhaile, A.S., Mitchell, N.C., Tempera, F., 2010. Development of volcanic insular
797 shelves: Insights from observations and modelling of Faial Island in the Azores Archipelago. Mar.
798 Geol. 275, 66-83.

799 Quartau, R., Trenhaile, A.S., Ramalho, R.S., Mitchell, N.C., 2018b. The role of subsidence in shelf
800 widening around ocean island volcanoes: Insights from observed morphology and modeling. Earth
801 Planet. Sci. Lett. 498, 408-417.

802 Ramalho, R.S., Helffrich, G., Madeira, J., Cosca, M., Thomas, C., Quartau, R., Hipólito, A., Rovere,
803 A., Hearty, P.J., Ávila, S.P., 2017. Emergence and evolution of Santa Maria Island (Azores)—The
804 conundrum of uplifted islands revisited. Geol. Soc. Am. Bull. 129, 372-390.

805 Ramalho, R.S., Quartau, R., Hóskuldsson, A., Madeira, J., Ventura da Cruz, J., Rodrigues, A., in
806 press. Evidence for late Pleistocene volcanism at Santa Maria Island, Azores? J Volcanol Geoth Res.

807 Ramalho, R.S., Quartau, R., Trenhaile, A.S., Mitchell, N.C., Woodroffe, C.D., Ávila, S.P., 2013.
808 Coastal evolution on volcanic oceanic islands: A complex interplay between volcanism, erosion,
809 sedimentation, sea-level change and biogenic production. Earth-Sci. Rev. 127, 140-170.

Ricchi, A., Quartau, R., Ramalho, R.S., Romagnoli, C., Casalbore, D., Ventura da Cruz, J., Fradique, C., Vinhas, A., 2018. Marine terraces development on reefless volcanic islands: new insights from high-resolution marine geophysical data offshore Santa Maria Island (Azores Archipelago). Mar. Geol. 406, 42-56.

Romagnoli, C., 2013. Characteristics and morphological evolution of the Aeolian volcanoes from the study of submarine portions, in: Lucchi, F., Peccerillo, A., Keller, J., Tranne, C.A., Rossi, P.L. (Eds.), Geological Society, London, Memoirs, 37, pp. 13-26.

Romagnoli, C., Belvisi, V., Innangi, S., Di Martino, G., Tonielli, R., 2020. New insights on the evolution of the Linosa volcano (Sicily Channel) from the study of its submarine portions. Marine Geology 419, 106060.

Romagnoli C., Casalbore D., Bosman A., Braga R., Chiocci F.L. (2013). Submarine structure of Vulcano Volcano (Aeolian Islands) revealed by high-resolution bathymetry and seismo-acoustic data. Marine Geology 338, 30–45.

Romagnoli, C., Casalbore, D., Chiocci, F.L., Bosman, A., 2009a. Offshore evidence of large-scale lateral collapses on the eastern flank of Stromboli, Italy, due to structurally-controlled, bilateral flank instability. Mar. Geol. 262, 1-13.

Romagnoli, C., Casalbore, D., Ricchi, A., Lucchi, F., Quartau, R., Bosman, A., Tranne, C.A., Chiocci, F.L., 2018. Morpho-bathymetric and seismo-stratigraphic analysis of the insular shelf of Salina (Aeolian archipelago) to unveil its Late-Quaternary geological evolution. Mar. Geol. 395, 133-151.

Romagnoli, C., Kokelaar, P., Casalbore, D., Chiocci, F.L., 2009b. Lateral collapses and active sedimentary processes on the northwestern flank of Stromboli volcano, Italy. Mar. Geol. 265, 101-119.

832 Rusu, L., Guedes Soares, C., 2012. Wave energy assessments in the Azores islands. Renew. Energy
833 45, 183-196.

834 Serralheiro, A., Alves, C.A.M., Forjaz, V.H., Rodrigues, B., 1987. Carta Vulcanológica dos Açores.
835 Ilha de Santa Maria na (folhas 1 e 2), scale 1:15,000. Serviço Regional de Protecção Civil dos
836 Açores, Universidade dos Açores and Centro de Vulcanologia, Ponta Delgada.

837 Serralheiro, A., Madeira, J., 1993. Stratigraphy and geochronology of Santa Maria Island (Azores).
838 Açoreana 7, 575-592.

839 Sibrant, A.L.R., Hildenbrand, A., Marques, F.O., Costa, A.C.G., 2015. Volcano-tectonic evolution of
840 the Santa Maria Island (Azores): Implications for paleostress evolution at the western Eurasia–
841 Nubia plate boundary. J. Volcanol. Geotherm. Res. 291, 49-62.

842 Taylor, B., 2019. Shoreline slope breaks revise understanding of Hawaiian shield volcanoes
843 evolution. Geochem. Geophys. Geosyst. 20, 4025-4045.

844 Thouret, J.C., 1999. Volcanic geomorphology-an overview. Earth-Sci. Rev. 47, 95-131.

845 Tsutsui, B., Campbell, J.F., Coulbourn, W.T., 1987. Storm-generated, episodic sediment movements
846 off Kahe Point, Oahu, Hawaii. Mar. Geol. 76, 281-299.

847 Uppala, S. M., P. Kållberg, A. Simmons, U. Andrae, V. d. Bechtold, M. Fiorino, J. Gibson, J. Haseler,
848 A. Hernandez, and G. Kelly., 2005. The ERA-40 re-analysis. Q. J. Roy. Meteor. Soc. 131 (612):2961-
849 3012.

850 Zbyszewski, G., Ferreira, O.V., 1960. Carta Geológica de Portugal—Ilha de Santa Maria (Açores),
851 scale 1:50,000. Serviços Geológicos de Portugal, Lisboa.

852 Zhao, Z., Mitchell, N.C., Quartau, R., Tempera, F. and Bricheno, L., 2019. Submarine Platform
853 Development by Erosion of a Surtseyan Cone at Capelinhos, Faial Island, Azores. Earth Surf. Proc.
854 Land. 44(15), 2982-3006.

855

856

857

858 Fig. 1. Shaded relief map illustrating the geodynamic setting of the islands (western, central and
859 eastern groups) in the Azores Archipelago (islands in white, Santa Maria Island in yellow) and how
860 they straddle the triple junction between the North American (NA), Eurasian (EU) and Nubian (NU)
861 lithospheric plates. MAR: Mid-Atlantic Ridge; PAR: Princess Alice Rift; EAFZ: Eastern Azores
862 Fracture Zone; TR: Terceira Rift; GF: Gloria Fault. Grey shading represents the deformation zone of
863 Terceira rift and dashed lines of the inactive Princess Alice Rift. The upper-right inset shows the
864 geographical setting of the Azores Archipelago within the Northern Atlantic Ocean. The
865 bathymetry is derived from the EMODNET web portal (http://portal.emodnet-bathymetry.eu/)
866 and tectonic structures adapted from Miranda et al. (2018).
867
868 Fig. 2. (a) Geological map of Santa Maria Island (modified after Ramalho et al., 2017), and (b)
869 WNW–ESE oriented cross-section. Underlying digital elevation model (DEM) is generated from a
870 1/5000 scale digital altimetric database from Secretaria Regional do Turismo e Transportes of the
871 Azores Government. Note that the Porto Formation is not visible on the map/section at this scale.
872
873 Fig. 3. Dataset used for this study, showing the seismic reflection profiles acquired during the
874 PLATMAR 1/2016 cruise. The multibeam survey covered the area shown by the seismic grid. Blue
875 dots represent location of sound speed profiles collected during the multibeam survey.
876 Bathymetry shown in this figure (~200m resolution) was derived from the EMODNET web portal
877 (http:// portal.emodnet-bathymetry.eu); topography is the same as the one shown in Figure 2.
878
879 Fig. 4. Shaded relief map of the multibeam bathymetry. Topography is the same as the one shown
880 in Figure 2.
881

Fig. 5. (a) Shaded relief map of the northern shelf sector showing the erosive shelf edge, headwalls scars, extension of tectonic features and volcanic cones. The seismic profile aa' is shown in Fig. 2ESM and seismic profiles bb' and cc' are shown in Fig. 3ESM. (b) Variation of shelf width and erosive shelf edge depth along the northern sector from west to east (from A to B). Shelf width was only measured on profiles perpendicular to the north coast.

Fig. 6. (a) Shaded relief map of the western shelf sector showing the erosive shelf edge, headwalls scars, and extension of tectonic features. The seismic profile dd' is shown in Fig. 4ESM (b) Variation of shelf width and erosive shelf edge depth along the western sector from north to south (from C to D).

Fig. 7. (a) Shaded relief map of the southern shelf sector showing the erosive shelf edge, headwalls scars, and extension of tectonic features. The seismic profiles ee', ff' and gg' are shown respectively in Figs. 5ESM, 6ESM and 7ESM (b) Variation of shelf width and erosive shelf edge depth along the southern sector from west to east (from E to F).

Fig. 8. (a) Shaded relief map of the eastern shelf sector showing the erosive shelf edge, headwalls scars, and extension of tectonic features. The seismic profiles hh' and ii' are shown in Figs. 8ESM and 9ESM, respectively. (b) Variation of shelf width and erosive shelf edge depth along the eastern sector from north to south (from G to H).

Fig. 9. Thickness map (in metres) of the unconsolidated sediments of the shelf surrounding Santa Maria Island.

906 Fig. 10. Offshore significant wave heights in the Santa Maria area derived from ERA 40 and ERA
907 Interim (Uppala et al., 2005; Dee et al., 2011)
908
909 Fig. 11. Reconstruction of the likely extension of the western shelf of Santa Maria Island 3.5 Ma
910 ago, before being partially raised. Color scale of topography is the same as Figure 3.

Table 1 – Extension of the rocky and sedimentary seafloor areas (in km^2 and %) of each shelf sector; measured volume of sediments in each sector; and ratio of volume of sediments of each shelf sector versus its total area.

Sectors	Area (km^2)			Area (%)		Volume of sediments (km^3)	Volume sediments/Total shelf area
	Sediments	Rocks	Total	Sediments	Rocks		
Northern	36.820	36.240	73.060	50.397	49.603	0.515	0.007
Western	3.300	9.900	13.200	25.000	75.000	0.037	0.003
Southern	9.450	9.580	19.030	49.658	50.342	0.221	0.012
Eastern	6.530	5.670	12.200	53.525	46.475	0.187	0.015

Electronic Supplementary Material

Fig. 1ESM. High resolution (1200 dpi) shaded relief map of the multibeam bathymetry. Topography is the same as the one shown in Figure 2.

Fig. 2ESM. Boomer seismic profile aa' showing the shelf morphology off the NW sector of Santa Maria. Location of the seismic profile in Figs. 5a and 9.

Fig. 3ESM. Boomer seismic profiles bb' and cc' showing the shelf morphology controlled by faults off the N and NE sector of Santa Maria. Location of the seismic profiles in Fig. 5a and 9.

Fig. 4ESM. Boomer seismic profile dd' showing the shelf morphology off the western sector of Santa Maria. Location of the seismic profile in Fig. 6a.

Fig. 5ESM. Boomer seismic profile ee' showing the shelf morphology off the southern sector of Santa Maria. Location of the seismic profile in Fig. 7a.

Fig. 6ESM. Boomer seismic profile ff' showing the shelf morphology controlled by faults off the southern sector of Santa Maria. Location of the seismic profile in Fig. 7a.

Fig. 7ESM. Boomer seismic profile gg' showing the shelf morphology off the southern sector of Santa Maria. Location of the seismic profile in Fig. 7a.

Fig. 8ESM. Boomer seismic profiles hh’ showing the shelf morphology off the eastern sector of Santa Maria. Location of the seismic profiles in Fig. 8a.

Fig. 9ESM. Boomer seismic profiles ii’ showing the the shelf morphology controlled by faults off the eastern sector of Santa Maria. Location of the seismic profiles in Fig. 8a.

Table 1ESM - Six hourly significant wave height H_s for the quadrant directions and respective frequencies derived from ERA 40 and ERA Interim for the period between 1957 and 2019 (Uppala et al., 2005; Dee et al., 2011).

Wave originating direction	Percent frequency (%) Significant wave height H_s (m)									Sum of percent frequency (%)	Average H_s (m)
	0 - 1 m	1 -2 m	2 - 3 m	3 - 4 m	4 - 5 m	5 - 6 m	6 - 7 m	7 - 8 m	>= 8 m		
N	0.99471	10.86626	5.20769	1.40490	0.32027	0.06699	0.02207	0.00590	0.00020	18.88899	1.922017
NE	0.56254	7.96483	2.96023	0.74180	0.15010	0.01982	0.00332	0.00111	0.00000	12.40375	1.830305
E	0.15145	2.15108	0.86000	0.29517	0.06035	0.00528	0.00000	0.00000	0.00000	3.52333	1.890301
SE	0.05794	0.67366	0.40322	0.13622	0.02203	0.00299	0.00000	0.00000	0.00000	1.29606	2.017559
S	0.09557	0.72673	0.59120	0.27056	0.05839	0.01118	0.00000	0.00000	0.00000	1.75363	2.204198
SW	0.19097	1.88260	1.55349	0.89456	0.34652	0.12226	0.02182	0.00577	0.00098	5.01897	2.453569
W	0.77025	8.88117	6.84695	3.62394	1.44261	0.54584	0.18249	0.06727	0.03071	22.39123	2.436865
NW	1.48884	17.00499	10.67882	3.78117	1.24923	0.35548	0.11542	0.03660	0.01347	34.72402	2.142374

Figure 1

Click here to access/download;Figure;Fig_1.jpg

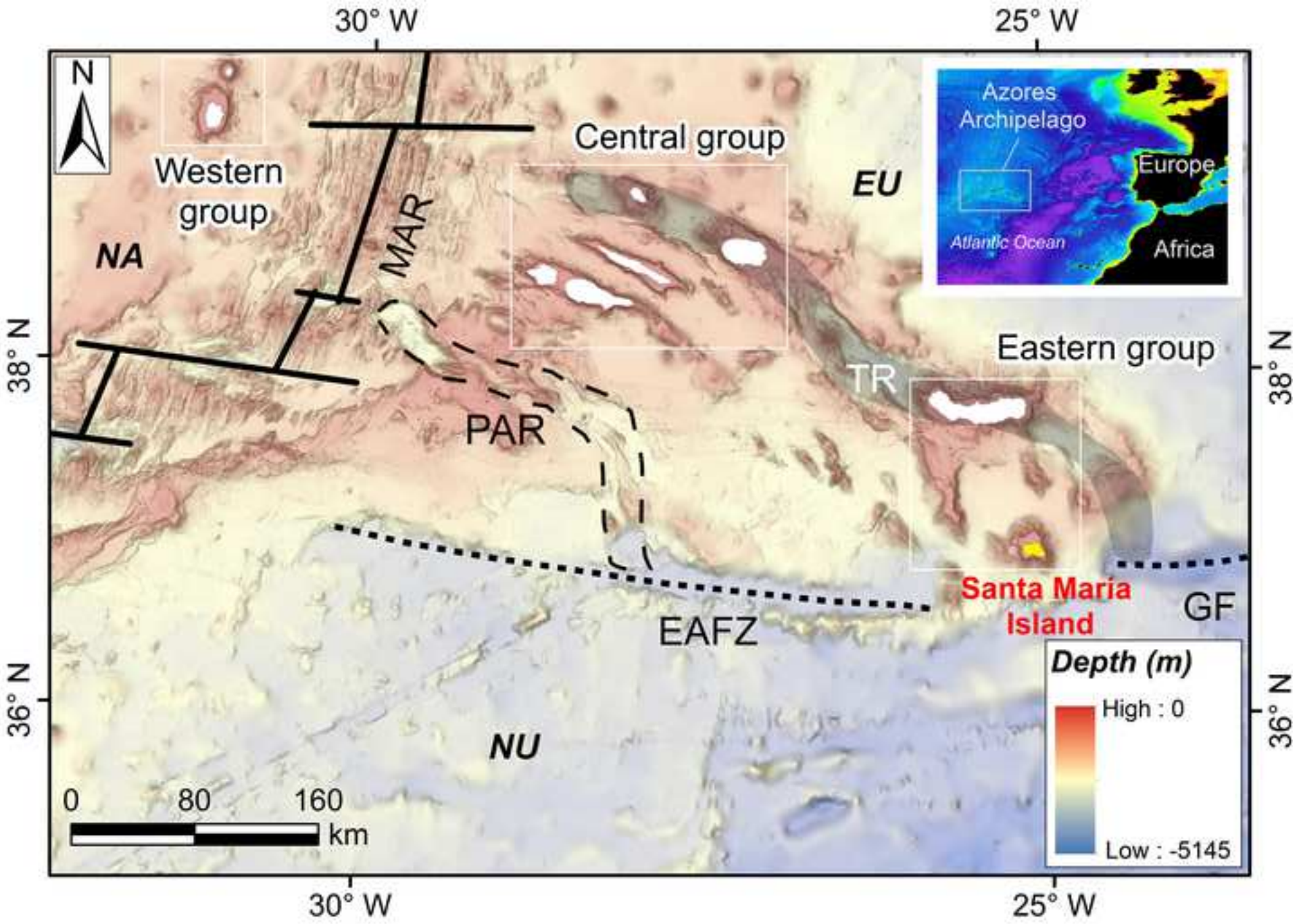

Figure 2

Click here to access/download;Figure;Fig_2.jpg

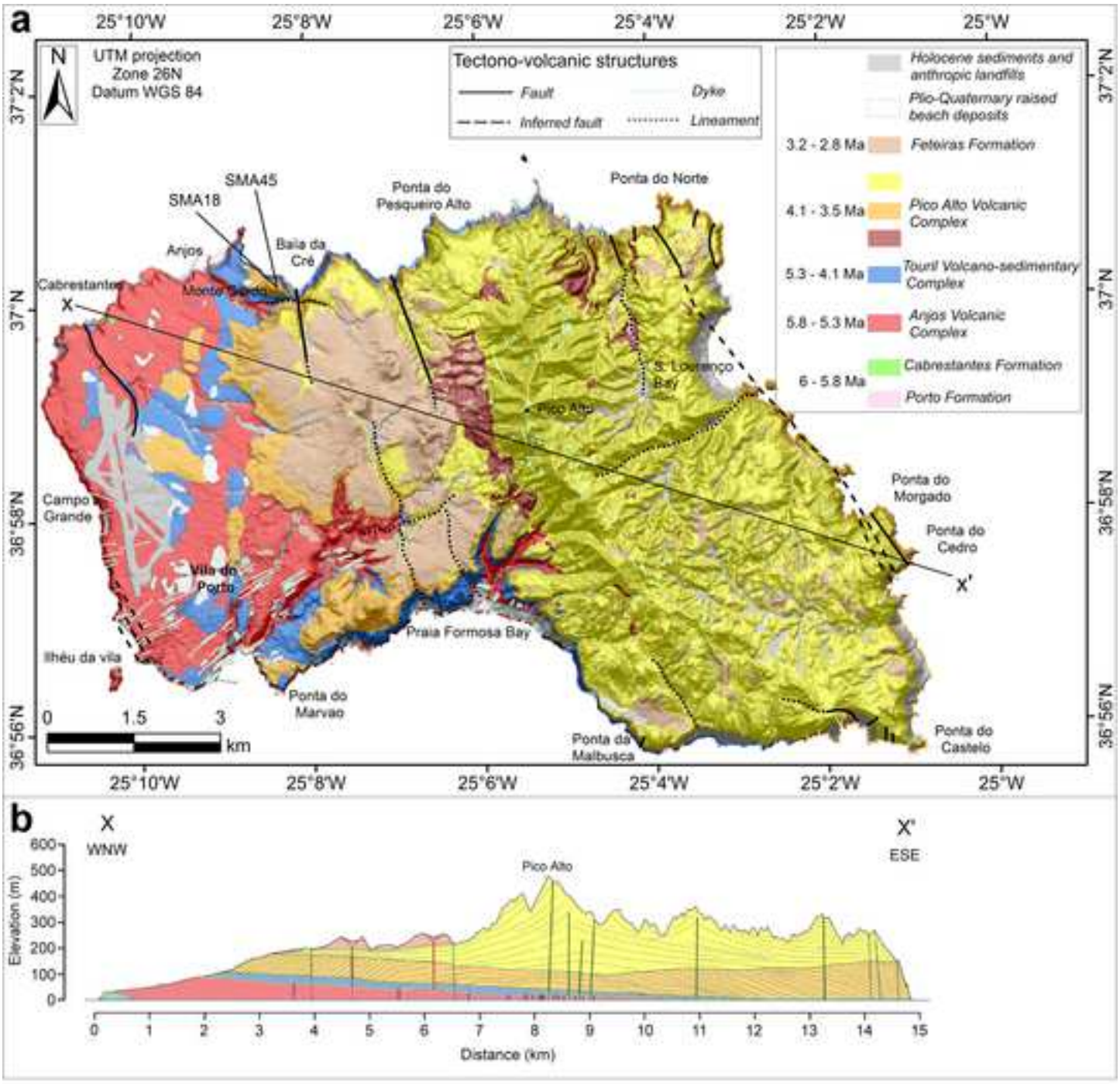

Figure 3

Click here to access/download;Figure;Fig_3.jpg

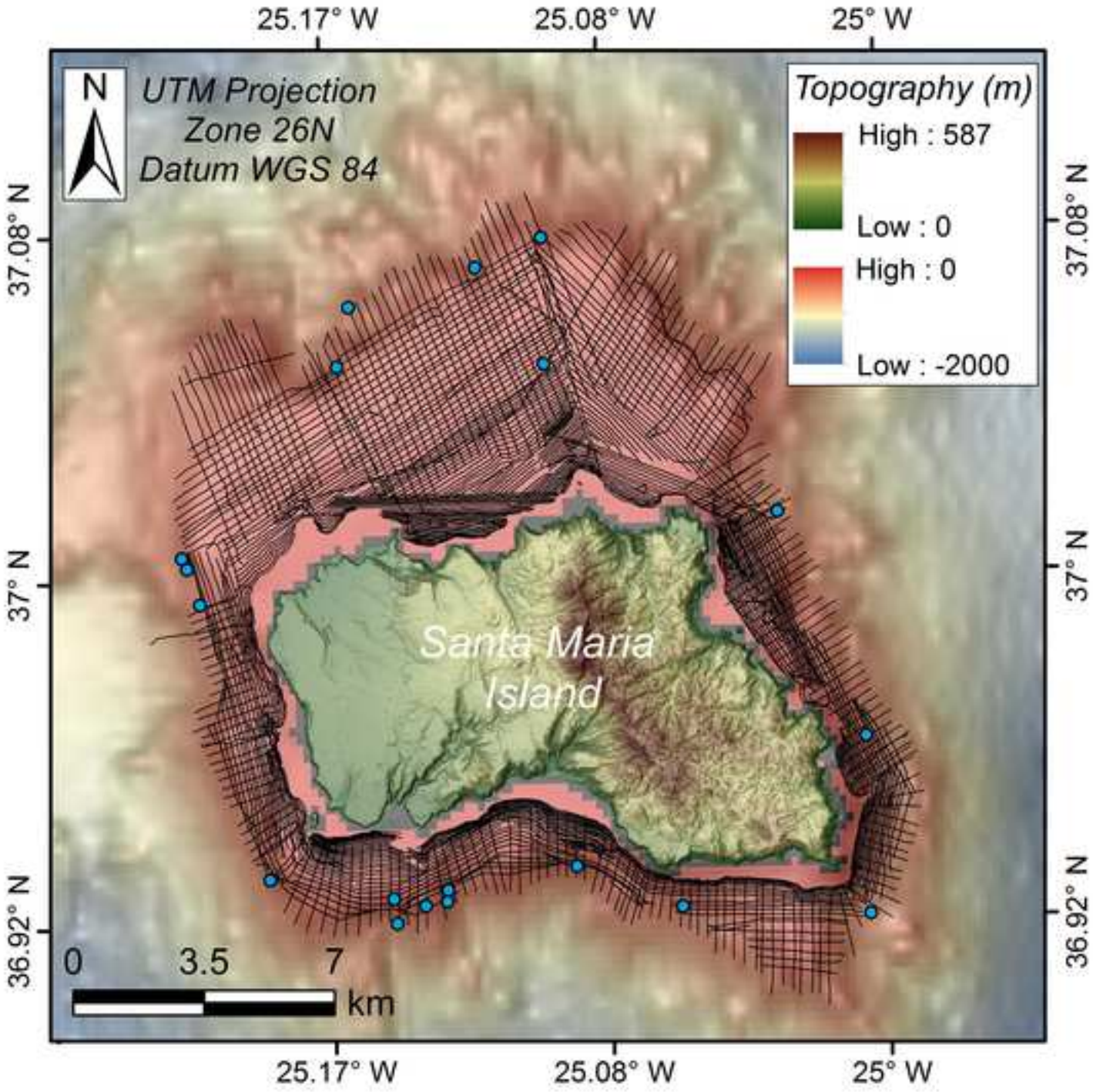

Figure 4

Click here to access/download;Figure;Fig_4.jpg

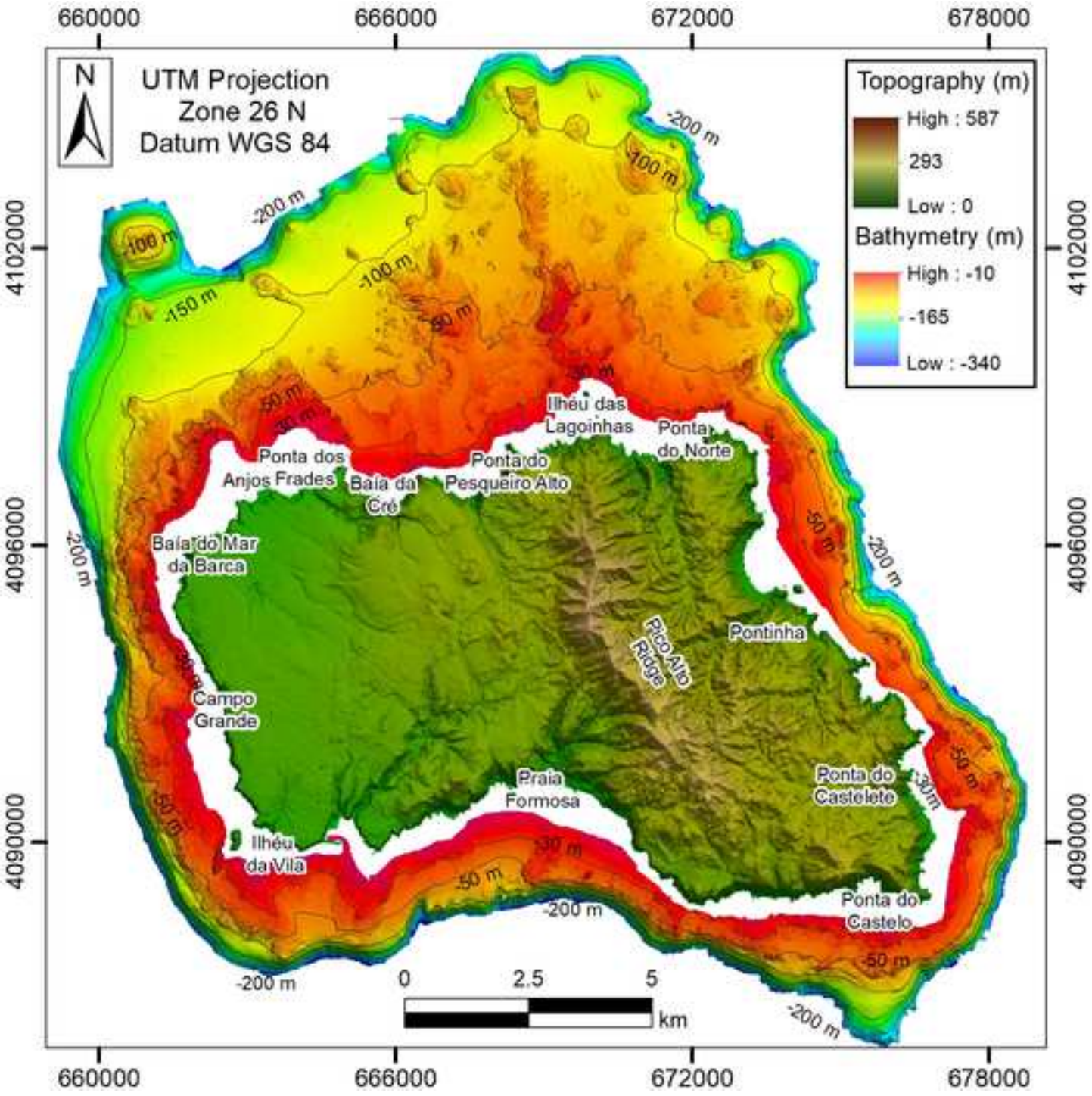

Figure 5

Click here to access/download;Figure;Fig_5.jpg

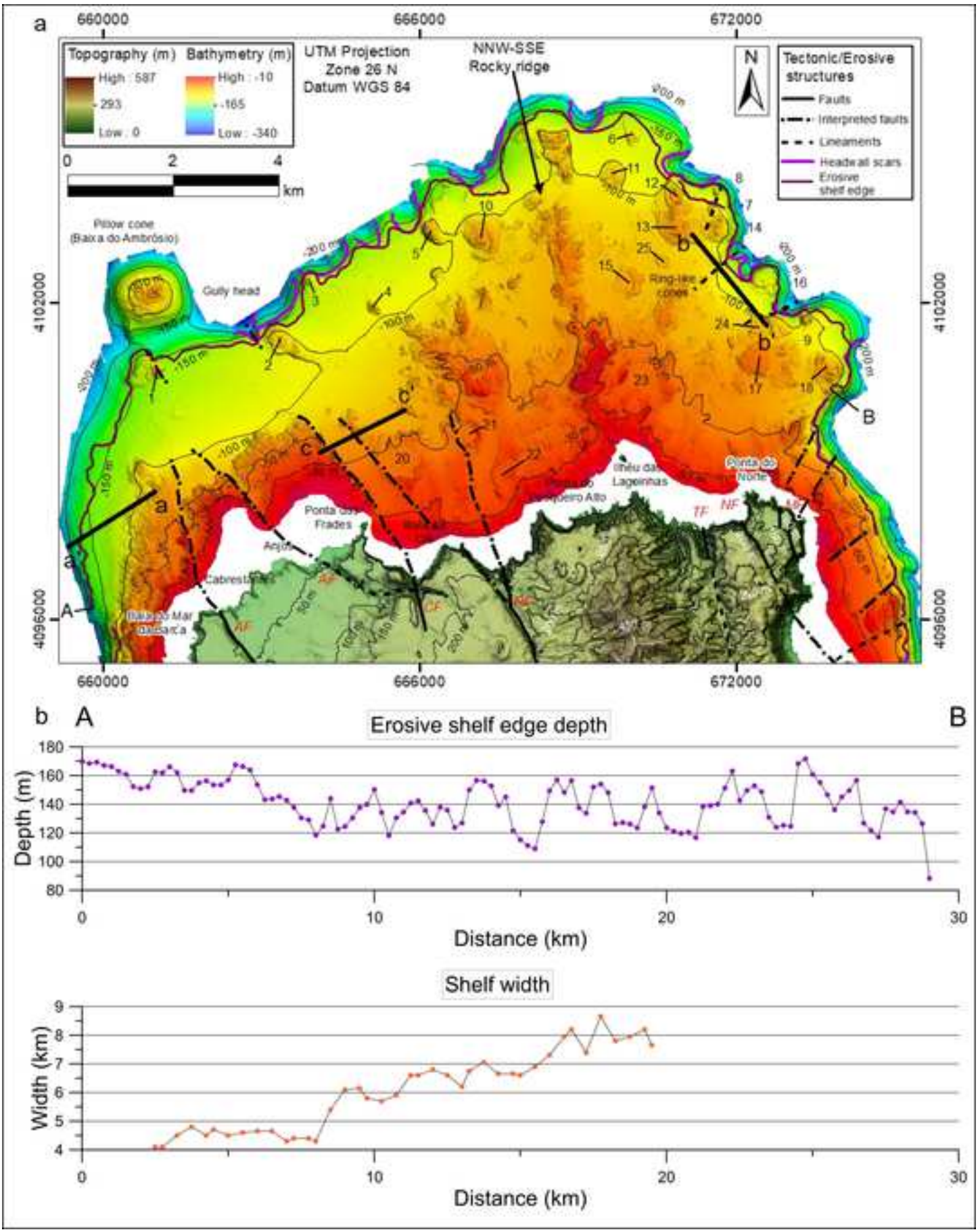

Figure 6

Click here to access/download;Figure;Fig_6.jpg

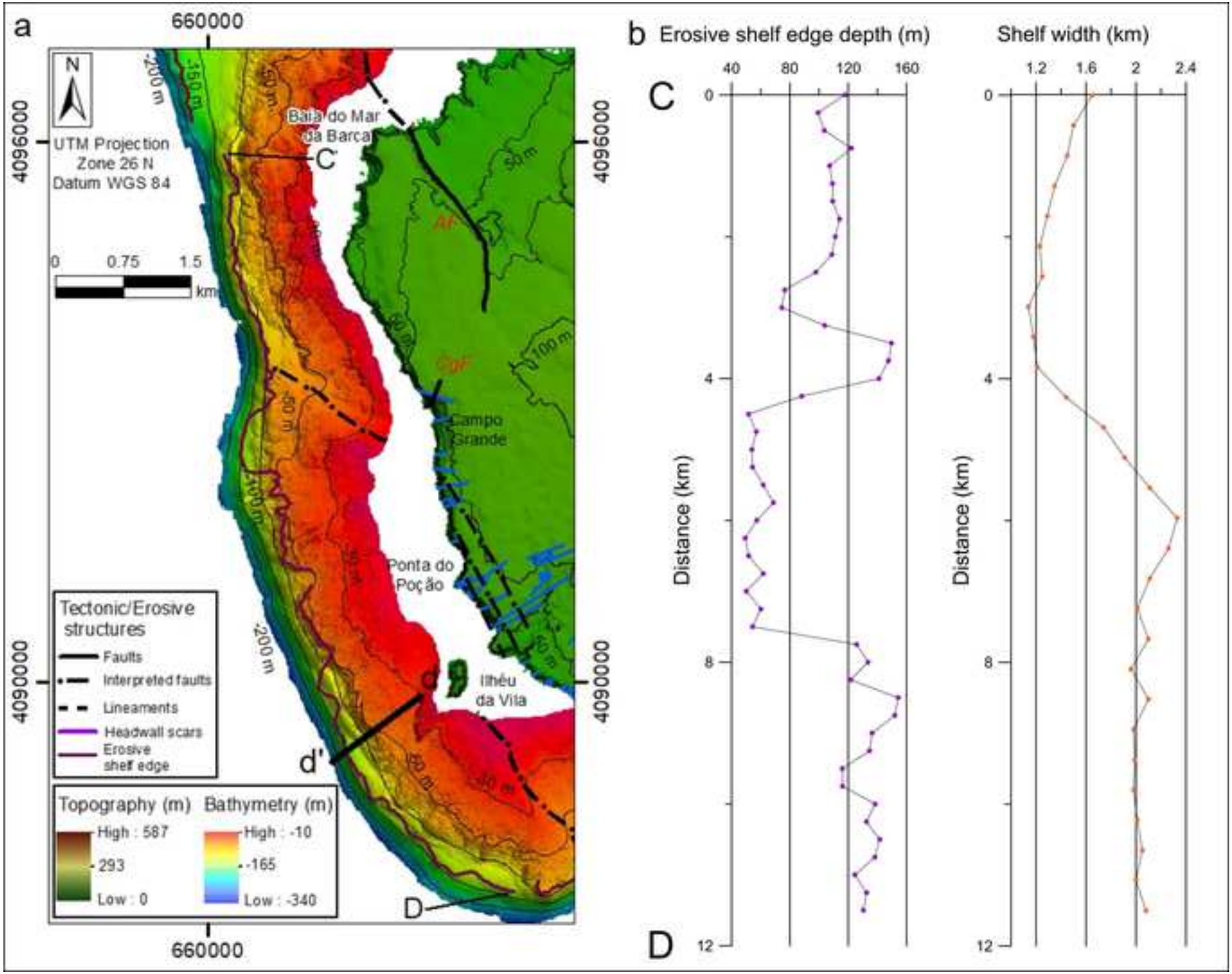

Figure 7

Click here to access/download;Figure;Fig_7.jpg

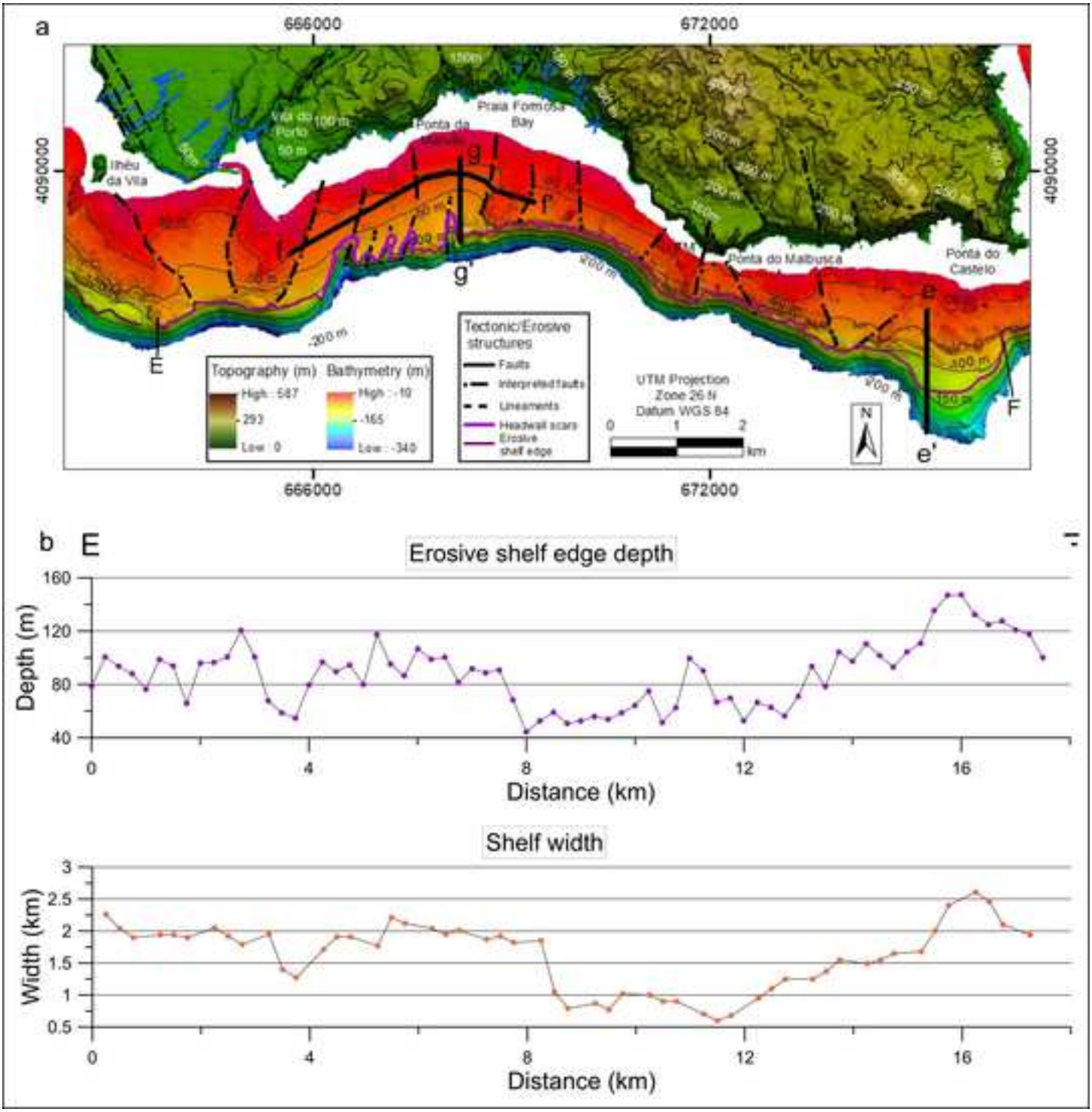

Figure 8

Click here to access/download;Figure;Fig_8.jpg

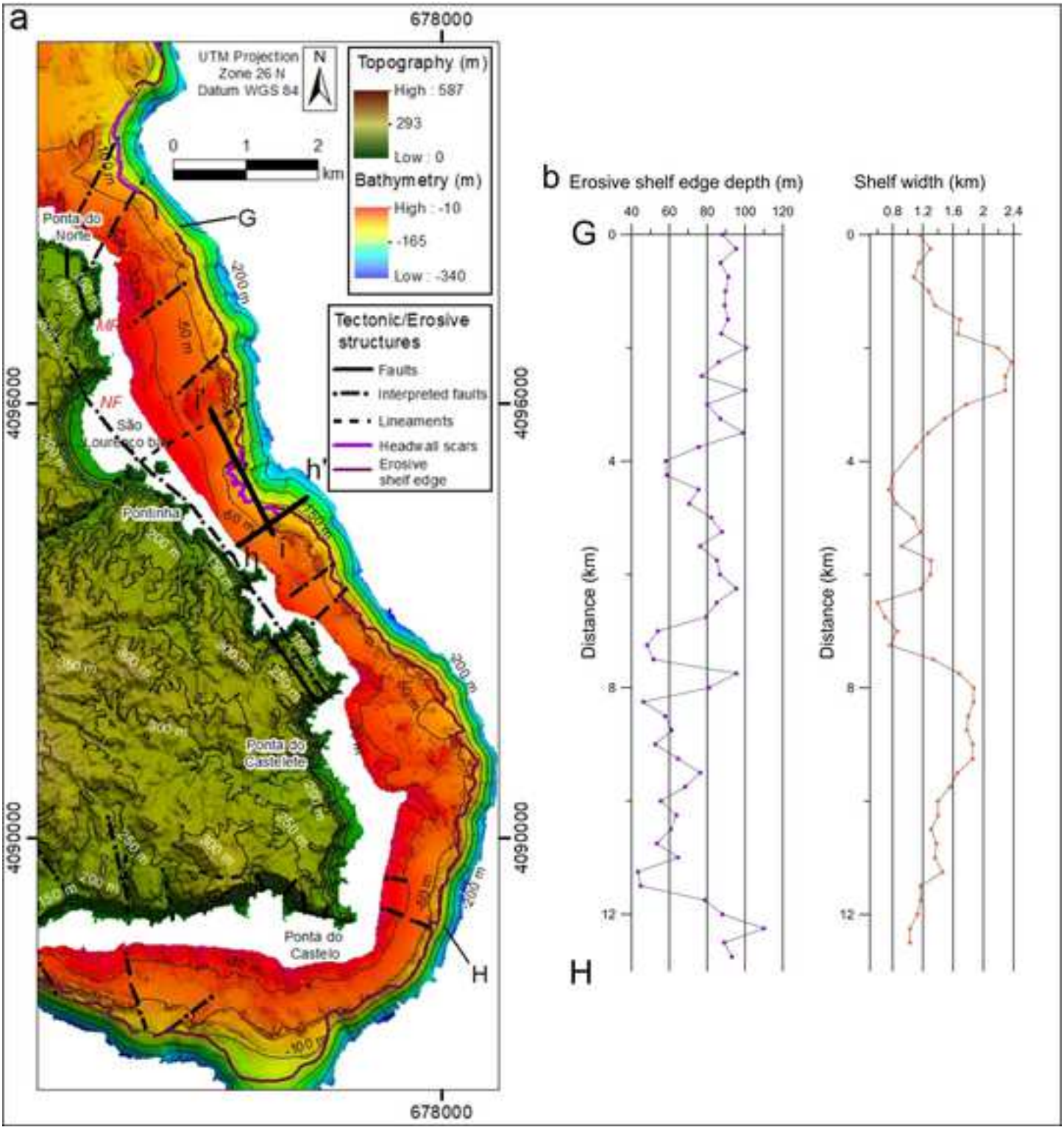

Figure 9

Click here to access/download;Figure;Fig_9.jpg

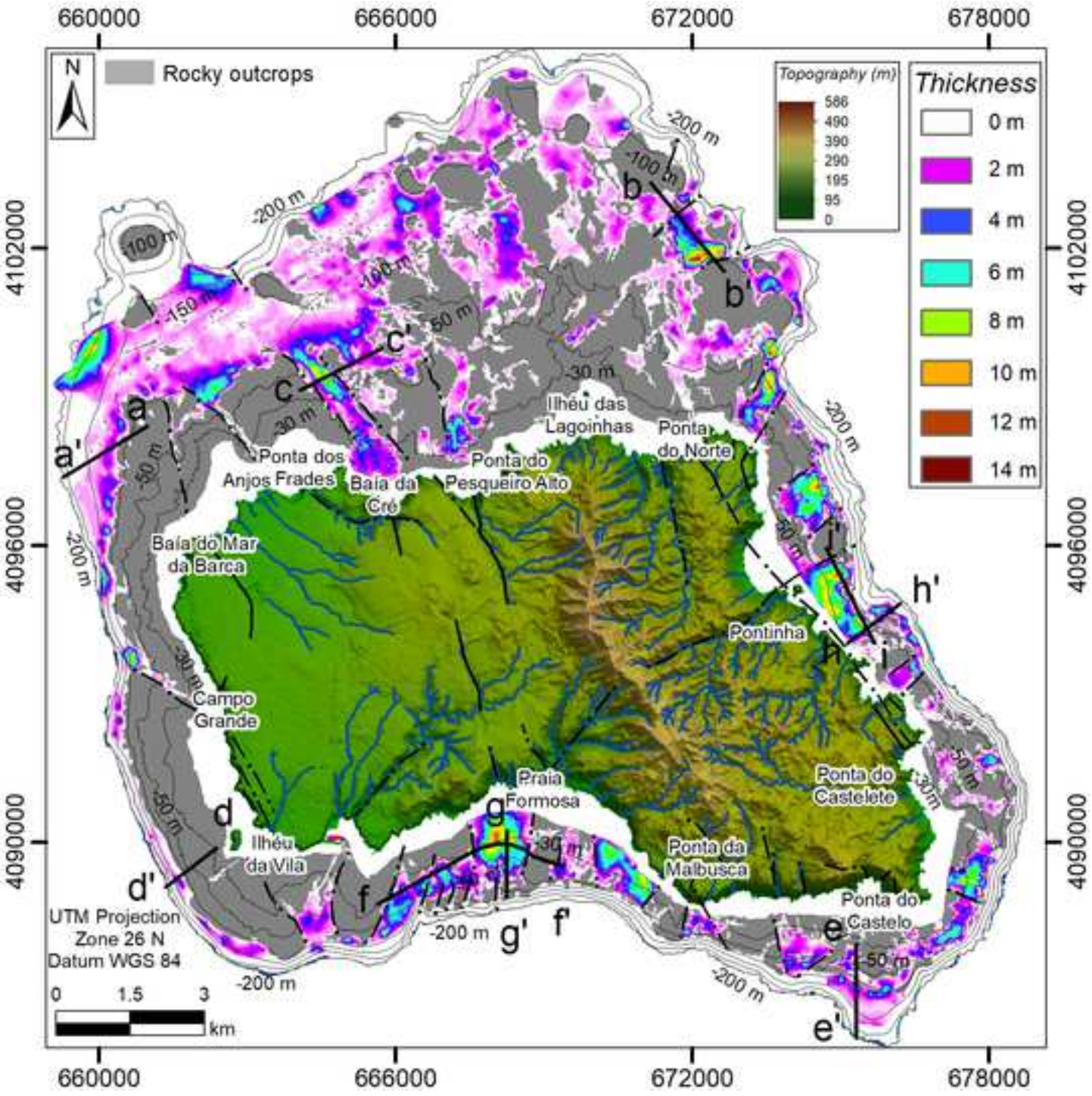

Figure 10

Click here to access/download;Figure;Fig_10.jpg

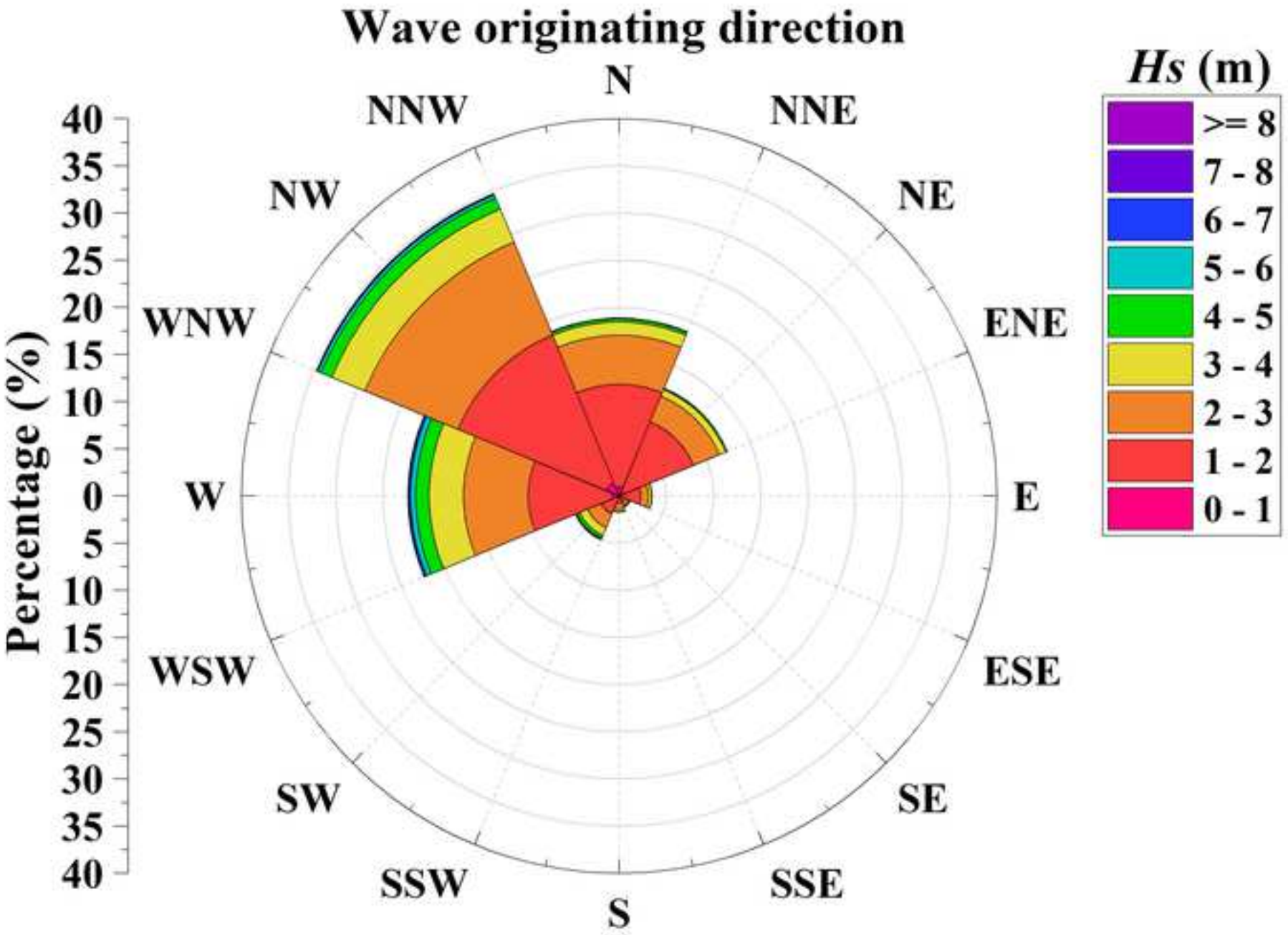

Figure 11

Click here to access/download;Figure;Fig_11.jpg

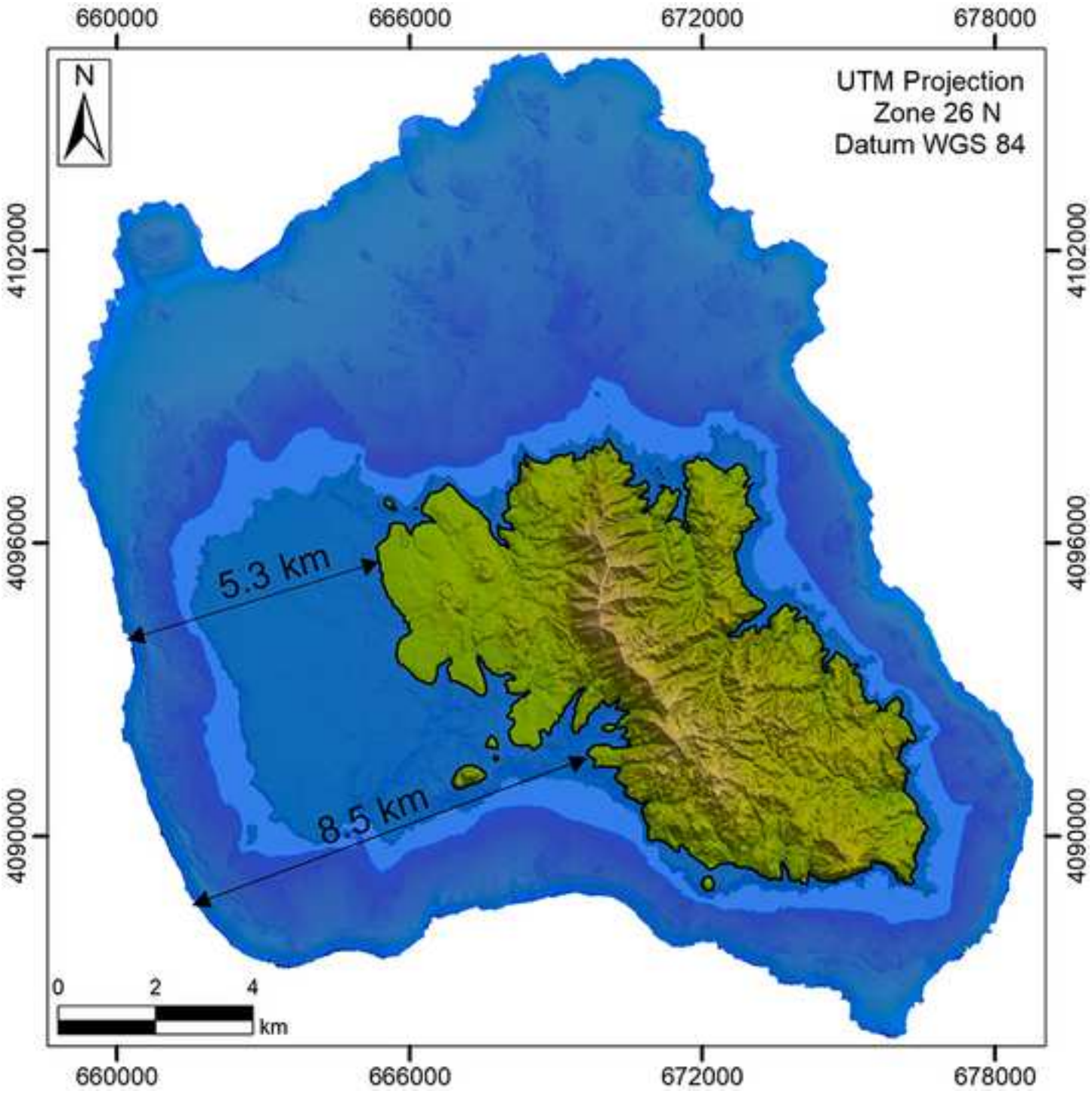

Figure 2ESM

Click here to access/download;Figure;Fig_2ESM.jpg

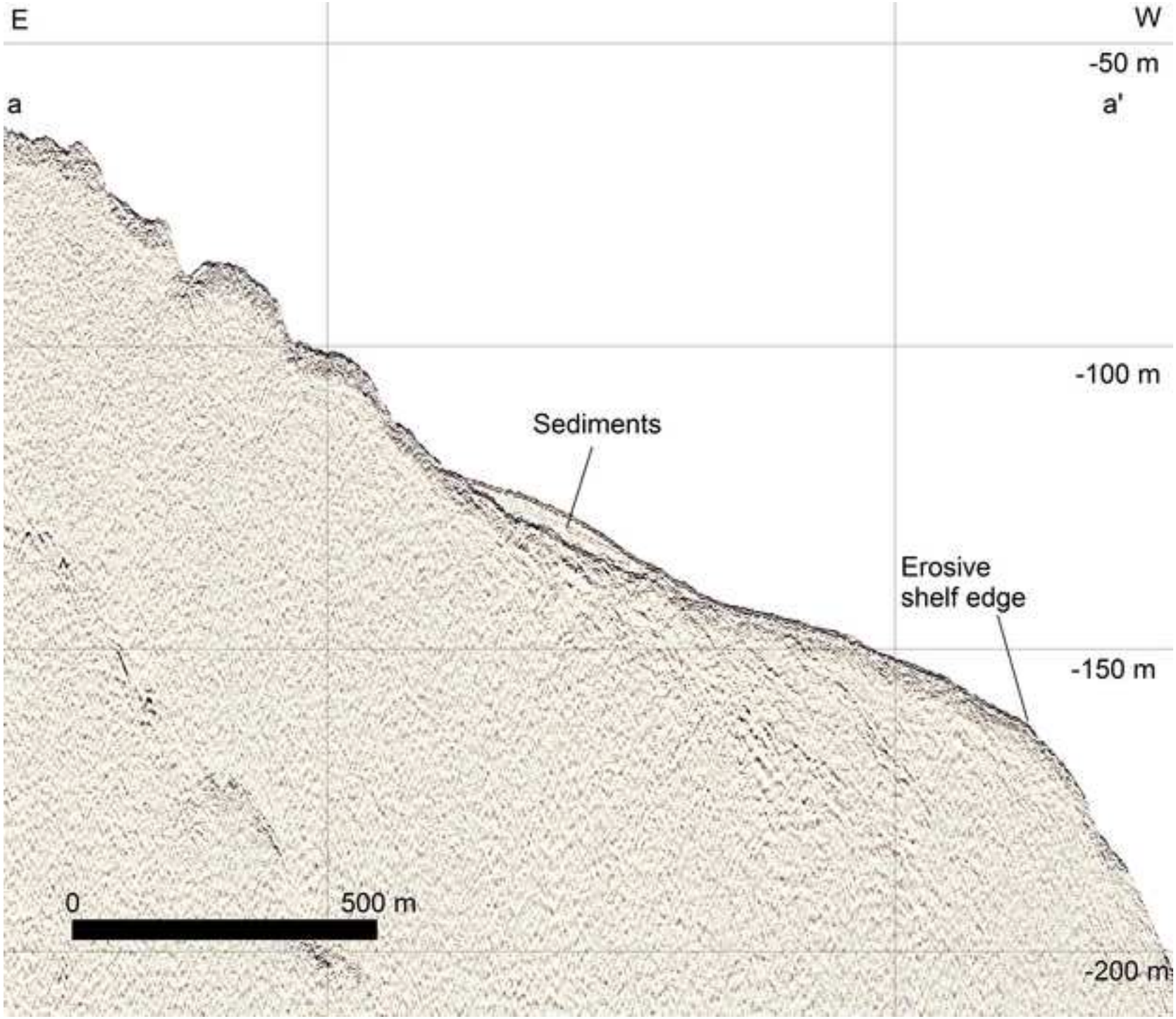

Figure 3ESM

Click here to access/download;Figure;Fig_3ESM.jpg

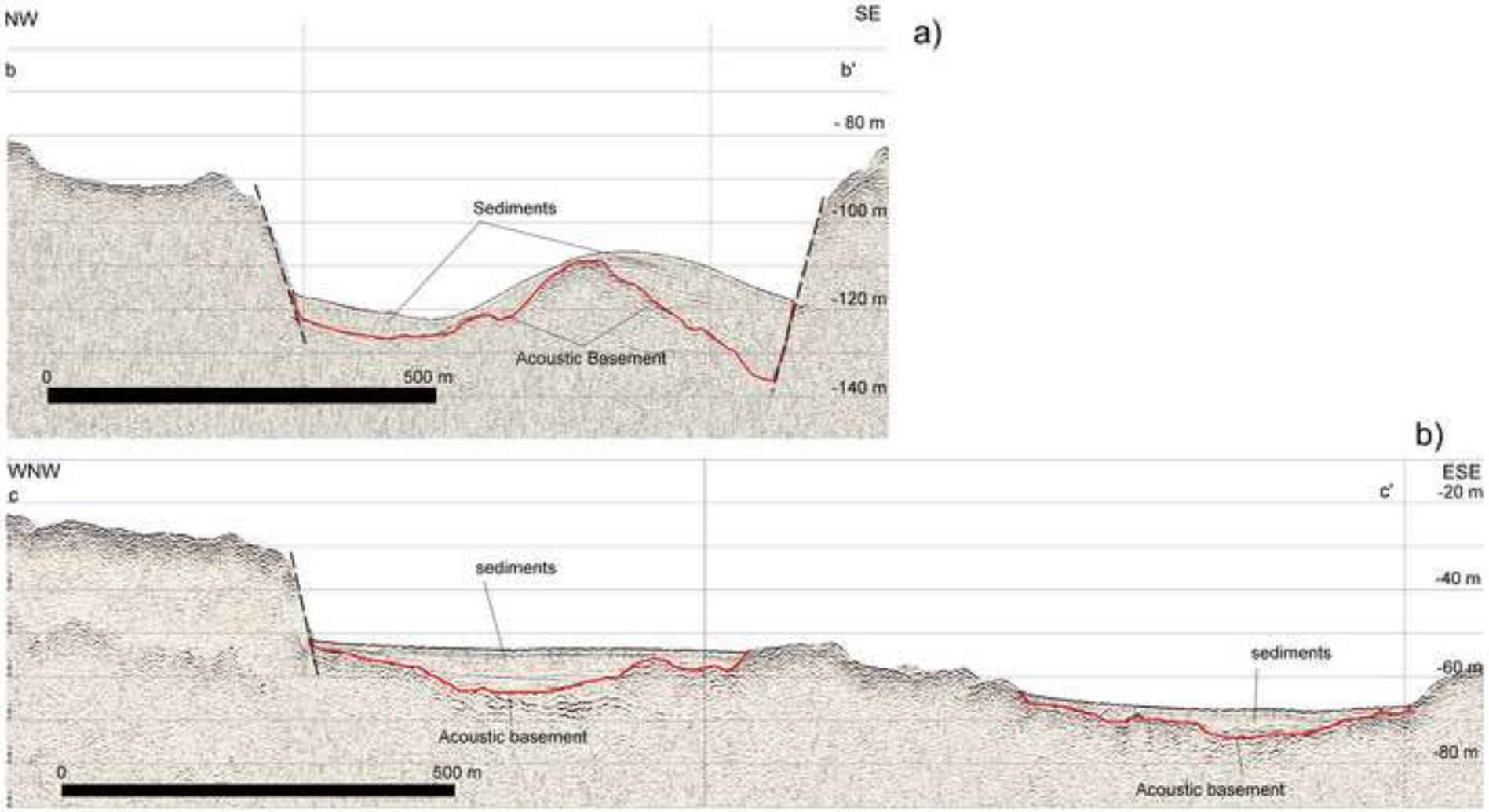

Figure 4ESM

Click here to access/download;Figure;Fig_4ESM.jpg

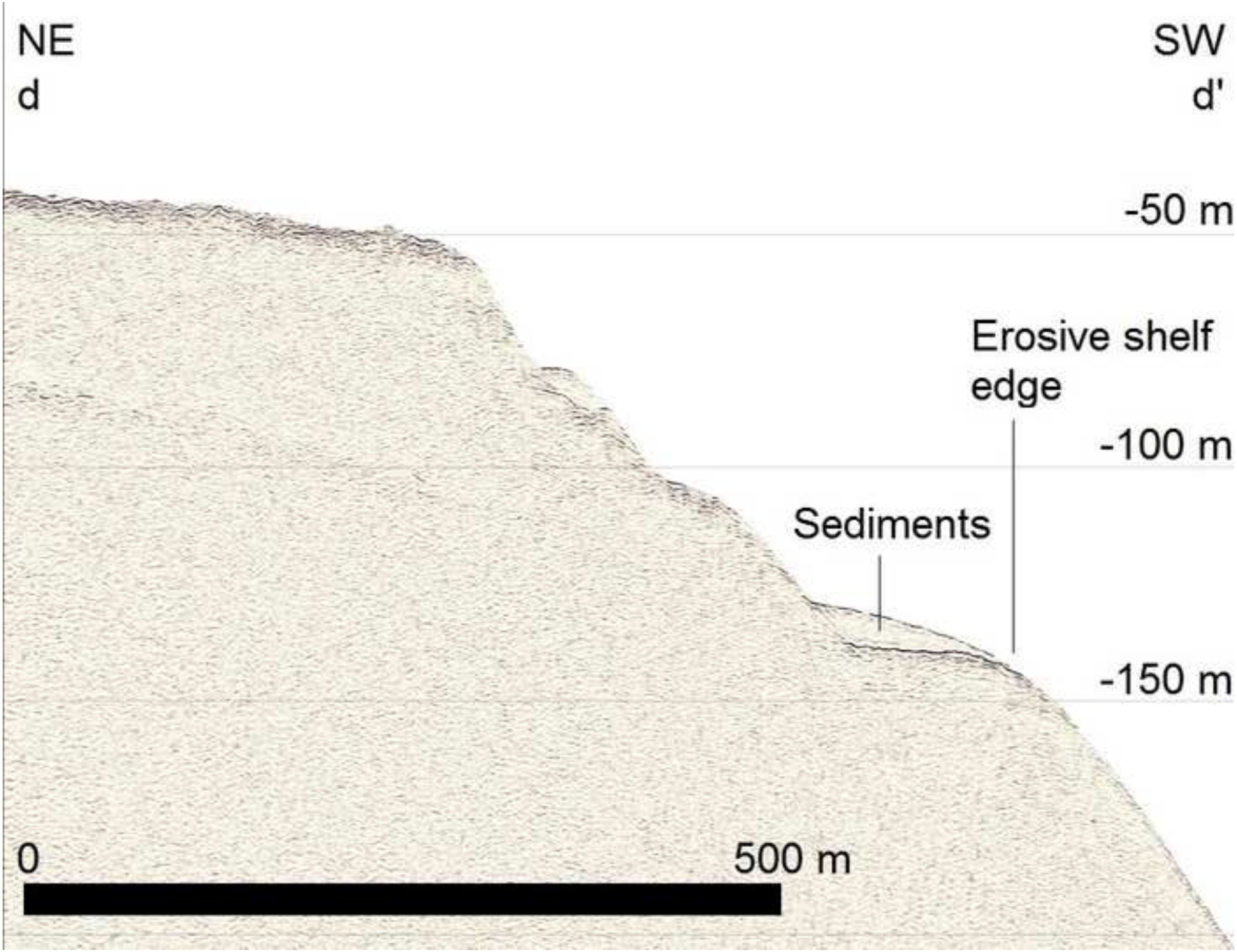

Figure 5ESM

Click here to access/download;Figure;Fig_5ESM.jpg

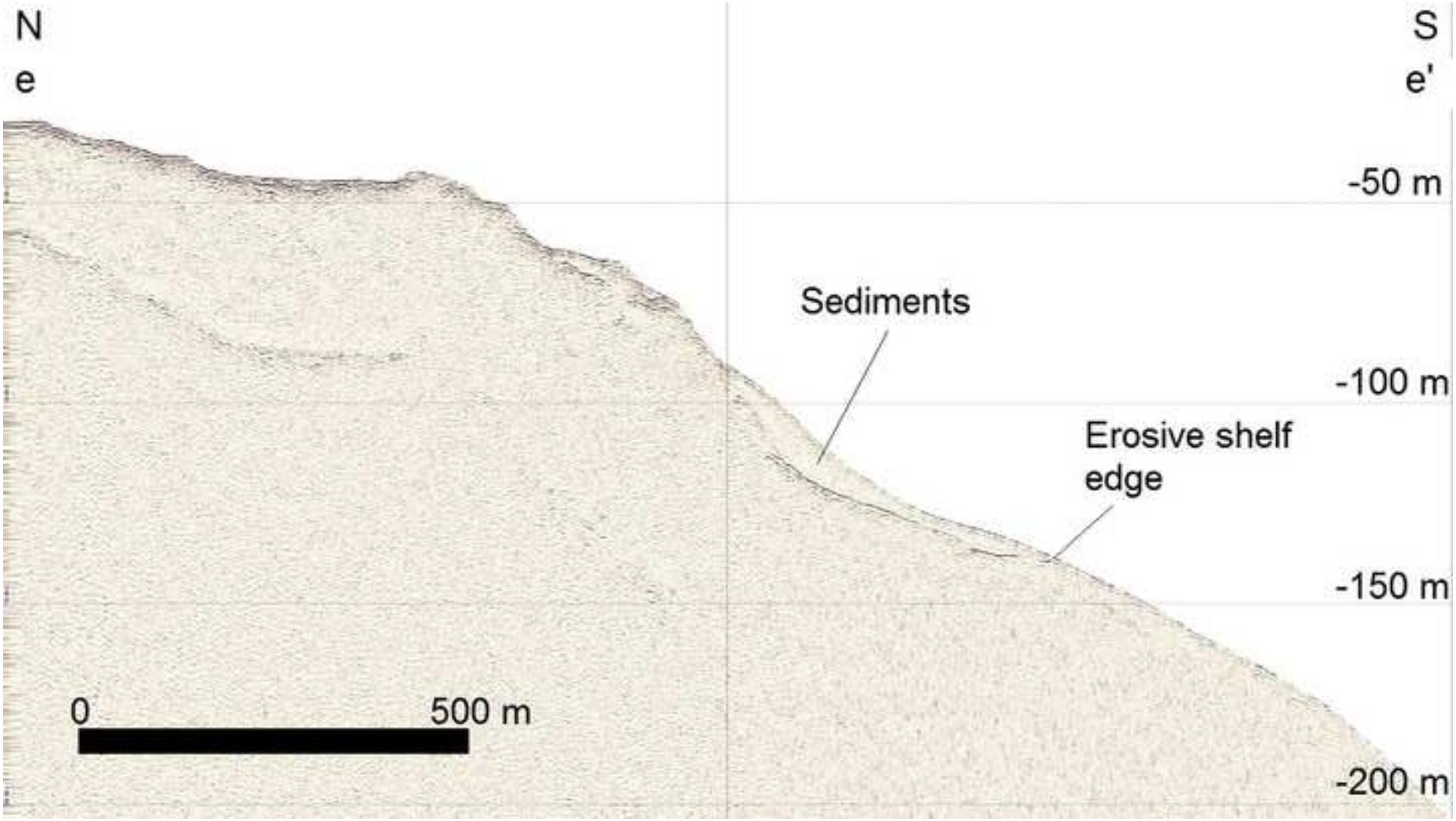

Figure 6ESM

Click here to access/download;Figure;Fig_6ESM.jpg

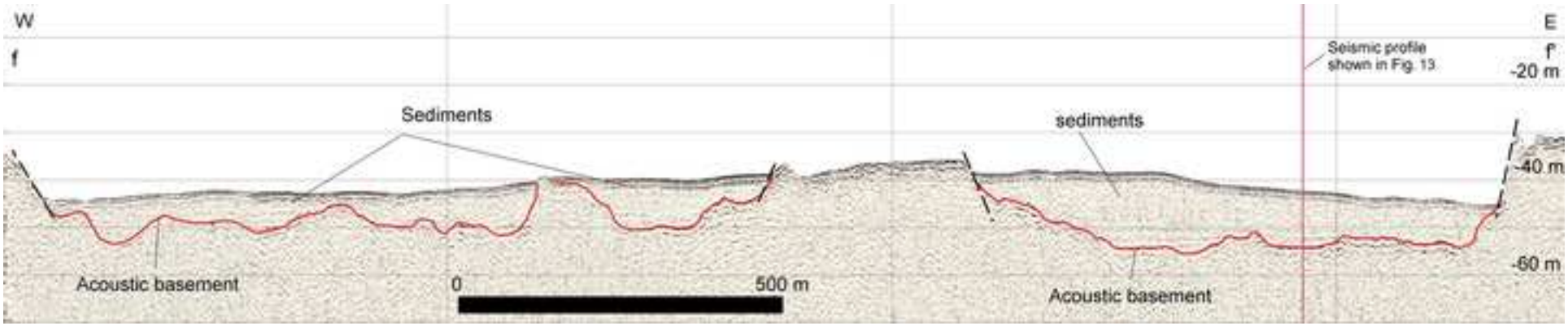

Figure 7ESM

Click here to access/download;Figure;Fig_7ESM.jpg

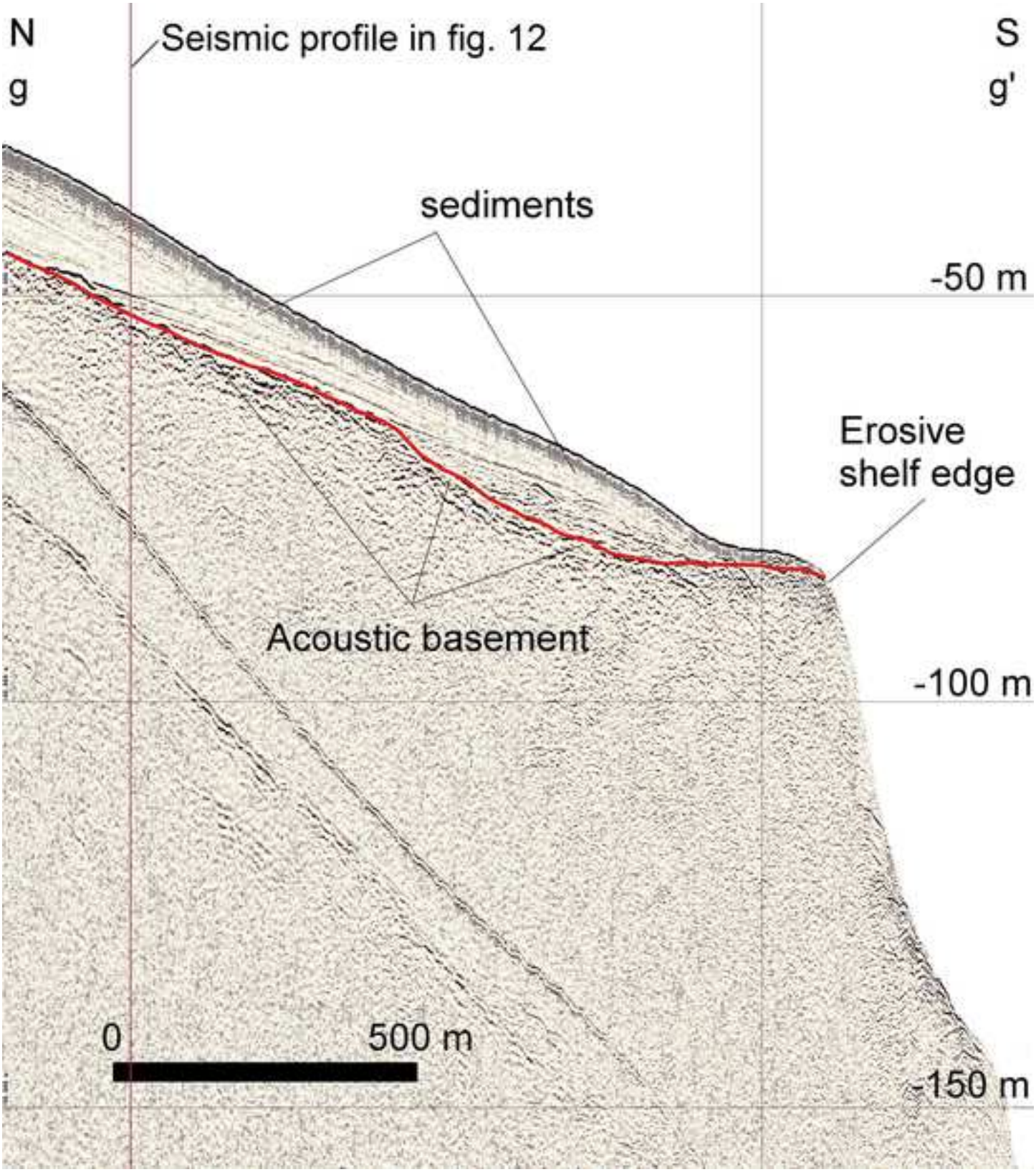

Figure 8ESM

Click here to access/download;Figure;Fig_8ESM.jpg

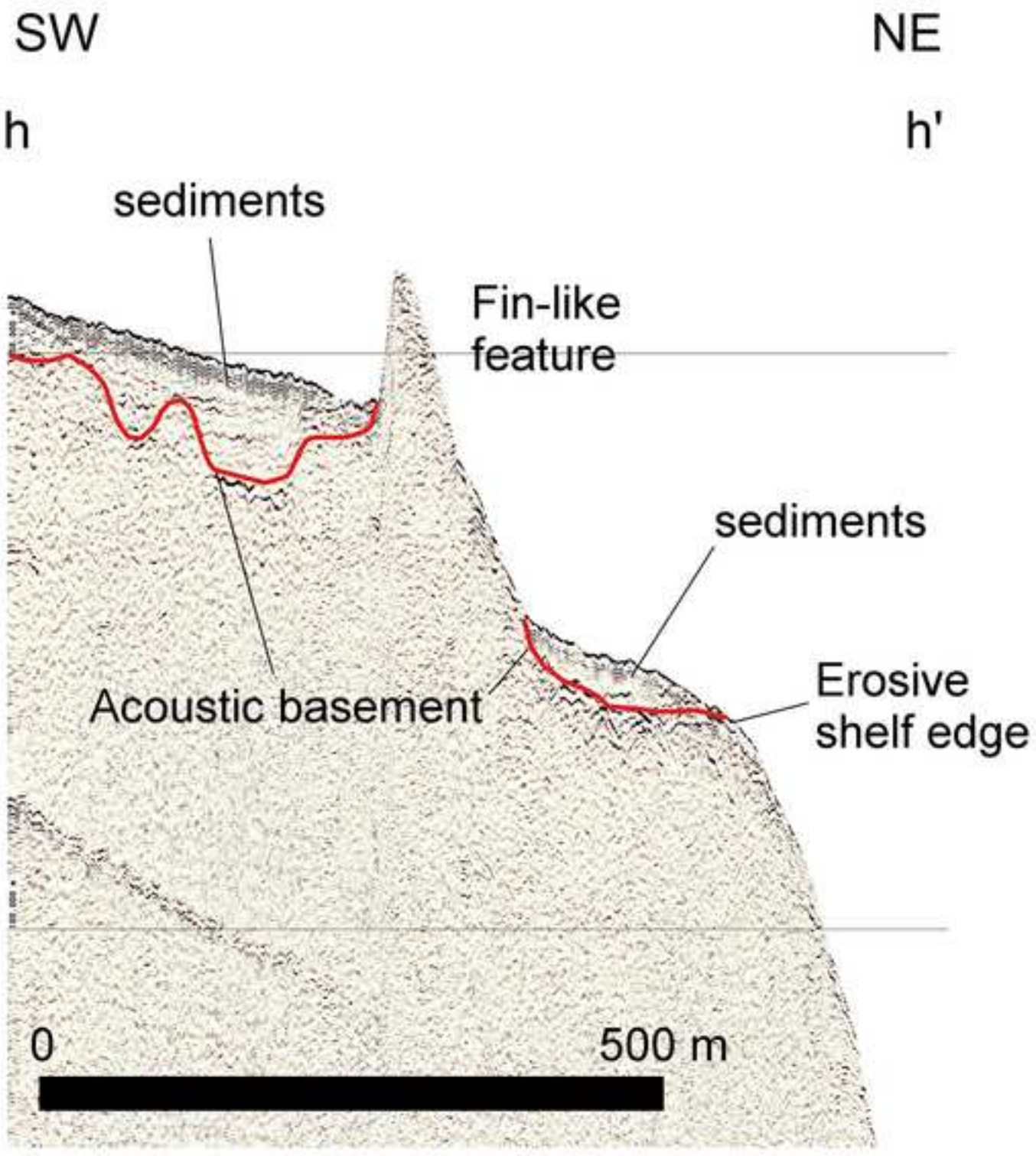

a)

Figure 9ESM

Click here to access/download;Figure;Fig_9ESM.jpg